

# UC Irvine

## UC Irvine Previously Published Works

### Title

Heterogeneity and chemical reactivity of the remote troposphere defined by aircraft measurements

### Permalink

<https://escholarship.org/uc/item/50t5n0wc>

### Journal

Atmospheric Chemistry and Physics, 21(18)

### ISSN

1680-7316

### Authors

Guo, Hao  
Flynn, Clare M  
Prather, Michael J  
[et al.](#)

### Publication Date

2021

### DOI

10.5194/acp-21-13729-2021

Peer reviewed



# Heterogeneity and chemical reactivity of the remote troposphere defined by aircraft measurements

Hao Guo<sup>1</sup>, Clare M. Flynn<sup>2</sup>, Michael J. Prather<sup>1</sup>, Sarah A. Strode<sup>3</sup>, Stephen D. Steenrod<sup>3</sup>, Louisa Emmons<sup>4</sup>, Forrest Lacey<sup>4,5</sup>, Jean-Francois Lamarque<sup>4</sup>, Arlene M. Fiore<sup>6</sup>, Gus Correa<sup>6</sup>, Lee T. Murray<sup>7</sup>, Glenn M. Wolfe<sup>3,8</sup>, Jason M. St. Clair<sup>3,8</sup>, Michelle Kim<sup>9</sup>, John Crouse<sup>10</sup>, Glenn Diskin<sup>10</sup>, Joshua DiGangi<sup>10</sup>, Bruce C. Daube<sup>11,12</sup>, Roisin Commane<sup>11,12</sup>, Kathryn McKain<sup>13,14</sup>, Jeff Peischl<sup>14,15</sup>, Thomas B. Ryerson<sup>13,15</sup>, Chelsea Thompson<sup>13</sup>, Thomas F. Hanisco<sup>3</sup>, Donald Blake<sup>16</sup>, Nicola J. Blake<sup>16</sup>, Eric C. Apel<sup>4</sup>, Rebecca S. Hornbrook<sup>4</sup>, James W. Elkins<sup>14</sup>, Eric J. Hintsa<sup>13,14</sup>, Fred L. Moore<sup>13,14</sup>, and Steven Wofsy<sup>11</sup>

<sup>1</sup>Department of Earth System Science, University of California, Irvine, CA 92697, USA

<sup>2</sup>Department of Meteorology, Stockholm University, Stockholm 106 91, Sweden

<sup>3</sup>Atmospheric Chemistry and Dynamics Laboratory, NASA Goddard Space Flight Center, Greenbelt, MD 20771, USA

<sup>4</sup>Atmospheric Chemistry Observations and Modeling Laboratory, National Center for Atmospheric Research, Boulder, CO 80301, USA

<sup>5</sup>Department of Mechanical Engineering, University of Colorado, Boulder, CO 80309, USA

<sup>6</sup>Department of Earth and Environmental Sciences and Lamont-Doherty Earth Observatory, Columbia University, Palisades, NY 10964, USA

<sup>7</sup>Department of Earth and Environmental Sciences, University of Rochester, Rochester, NY 14611, USA

<sup>8</sup>Joint Center for Earth Systems Technology, University of Maryland, Baltimore County, Baltimore, MD 21228, USA

<sup>9</sup>Department of Geological and Planetary Sciences, California Institute of Technology, Pasadena, CA 91125, USA

<sup>10</sup>Atmospheric Composition, NASA Langley Research Center, Hampton, VA 23666, USA

<sup>11</sup>John A. Paulson School of Engineering and Applied Sciences, Harvard University, Cambridge, MA 02138, USA

<sup>12</sup>Department of Earth and Planetary Sciences, Harvard University, Cambridge, MA 02138, USA

<sup>13</sup>Cooperative Institute for Research in Environmental Sciences, University of Colorado, Boulder, CO 80309, USA

<sup>14</sup>Global Monitoring Division, Earth System Research Laboratory, NOAA, Boulder, CO 80305, USA

<sup>15</sup>Chemical Sciences Division, National Oceanic and Atmospheric Administration Earth System Research Laboratory, Boulder, CO 80305, USA

<sup>16</sup>Department of Chemistry, University of California, Irvine, CA 92697, USA

**Correspondence:** Hao Guo (haog2@uci.edu) and Michael J. Prather (mprather@uci.edu)

Received: 13 May 2021 – Discussion started: 19 May 2021

Revised: 20 August 2021 – Accepted: 24 August 2021 – Published: 16 September 2021

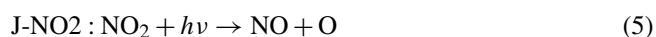
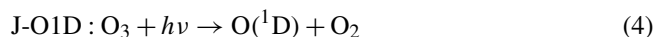
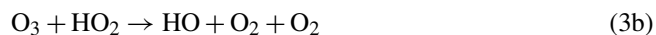
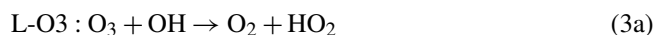
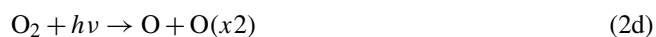
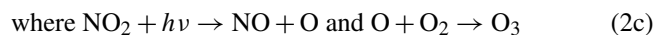
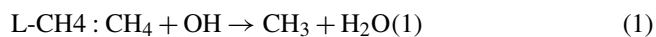
**Abstract.** The NASA Atmospheric Tomography (ATom) mission built a photochemical climatology of air parcels based on in situ measurements with the NASA DC-8 aircraft along objectively planned profiling transects through the middle of the Pacific and Atlantic oceans. In this paper we present and analyze a data set of 10 s (2 km) merged and gap-filled observations of the key reactive species driving the chemical budgets of O<sub>3</sub> and CH<sub>4</sub> (O<sub>3</sub>, CH<sub>4</sub>, CO, H<sub>2</sub>O, HCHO, H<sub>2</sub>O<sub>2</sub>, CH<sub>3</sub>OOH, C<sub>2</sub>H<sub>6</sub>, higher alkanes, alkenes, aromatics, NO<sub>x</sub>, HNO<sub>3</sub>, HNO<sub>4</sub>, peroxyacetyl nitrate, other

organic nitrates), consisting of 146 494 distinct air parcels from ATom deployments 1 through 4. Six models calculated the O<sub>3</sub> and CH<sub>4</sub> photochemical tendencies from this modeling data stream for ATom 1. We find that 80 %–90 % of the total reactivity lies in the top 50 % of the parcels and 25 %–35 % in the top 10 %, supporting previous model-only studies that tropospheric chemistry is driven by a fraction of all the air. In other words, accurate simulation of the least reactive 50 % of the troposphere is unimportant for global budgets. Surprisingly, the probability densities of species and reactiv-

ities averaged on a model scale (100 km) differ only slightly from the 2 km ATom data, indicating that much of the heterogeneity in tropospheric chemistry can be captured with current global chemistry models. Comparing the ATom reactivities over the tropical oceans with climatological statistics from six global chemistry models, we find excellent agreement with the loss of O<sub>3</sub> and CH<sub>4</sub> but sharp disagreement with production of O<sub>3</sub>. The models sharply underestimate O<sub>3</sub> production below 4 km in both Pacific and Atlantic basins, and this can be traced to lower NO<sub>x</sub> levels than observed. Attaching photochemical reactivities to measurements of chemical species allows for a richer, yet more constrained-to-what-matters, set of metrics for model evaluation.

## 1 Prologue

This paper is based on the methods and results of papers that established an approach for analyzing aircraft measurements, specifically the NASA Atmospheric Tomography Mission (ATom), with global chemistry models. Here we present a brief overview of those papers to help the reader understand the basis for this paper. The first ATom modeling paper (“Global atmospheric chemistry – which air matters”, Prather et al., 2017, hence P2017) gathered six global models, both chemistry–transport models (CTMs) and chemistry–climate models (CCMs). The models reported a single-day snapshot for mid-August (the time of the first ATom deployment, ATom-1), and these included all species relevant for tropospheric chemistry and the 24 h reactivities. We limited our study to three reactivities (Rs) controlling methane (CH<sub>4</sub>) and tropospheric ozone (O<sub>3</sub>) using specific reaction rates to define the loss of CH<sub>4</sub> and the production and loss of O<sub>3</sub> in parts per billion (ppb) per day. The critical photolysis rates (*J* values) are also reported as 24 h averages.



Models also reported the change in O<sub>3</sub> over 24 h, and these match the P-O3 minus L-O3 values over the Pacific basin (a focus of this study). The models showed a wide range in the three Rs average profiles across latitudes over the Pacific basin, as well as 2D probability densities (PDs) for key species such as NO<sub>x</sub> (NO + NO<sub>2</sub>) versus HOOH. A large part of the model differences was attributed to the large differences found in chemical composition. We found that single transects from a model through the tropical Pacific at different longitudes produced nearly identical 2D PDs, but these PDs were distinctly different across models. This result supported the premise that the ATom PDs would provide a useful metric for global chemistry models.

In P2017, we established a method for running the chemistry modules in the CTMs and CCMs with an imposed chemical composition from aircraft data: the ATom run, or “A run”. In the A run, the chemistry of each grid cell does not interact with its neighbors or with externally imposed emission sources. Effectively the CTM/CCM is initialized and run for 24 h without transport, scavenging or emissions. Aerosol chemistry is also turned off in the A runs. This method allows each parcel to evolve in response to the daily cycle of photolysis in each model and be assigned a 24 h integrated reactivity. The instantaneous reaction rates at the time an air parcel is measured (e.g., near sunset at the end of a flight) do not reflect that parcel’s overall contribution to the CH<sub>4</sub> or O<sub>3</sub> budget; a full diel cycle is needed. The A run assumption that parcels do not mix with neighboring air masses is an approximation, and thus for each model we compared the A runs using the model’s restart data with a parallel standard 24 h simulation (including transport, scavenging, and emissions). Because the standard grid-cell air moves and mixes, we compared averages over a large region (e.g., tropical Pacific). We find some average biases of order ±10 % but general agreement. The largest systematic biases in the A runs are caused by buildup of HOOH (no scavenging) and decay of NO<sub>x</sub> (no sources). The A runs are relatively easy to code for most CTM/CCMs and allow each model’s chemistry module, including photolysis package, to run normally. The A runs do not distinguish between CTMs and CCMs, except that each model will generate/prescribe its own cloud fields and photolysis rates. Our goal is to create a robust understanding of the chemical statistics including the reactivities with which to test and evaluate the free-running CCMs, and thus we do not try to model the specific period of the ATom deployments. Others may use the ATom data with hindcast CTMs to test forecast models, but here we want to build a chemical climatology.

The first hard test of the A runs came with the second ATom modeling paper (“How well can global chemistry models calculate the reactivity of short-lived greenhouse gases in the remote troposphere, knowing the chemical composition”, Prather et al., 2018, hence P2018). The UCI CTM simulated an aircraft-like data set of 14 880 air parcels along the International Date Line from a separate high-resolution

(0.5°) model. Each parcel is defined by the following core species: H<sub>2</sub>O, O<sub>3</sub>, NO<sub>x</sub>, HNO<sub>3</sub>, HNO<sub>4</sub>, PAN (peroxyacetyl nitrate), CH<sub>3</sub>NO<sub>3</sub>, HOOH, CH<sub>3</sub>OOH, HCHO, CH<sub>3</sub>CHO (acetaldehyde), C<sub>3</sub>H<sub>6</sub>O (acetone), CO, CH<sub>4</sub>, C<sub>2</sub>H<sub>6</sub>, alkanes (C<sub>3</sub>H<sub>8</sub> and higher), C<sub>2</sub>H<sub>4</sub>, aromatics (benzene, toluene, xylene) and C<sub>5</sub>H<sub>8</sub> (isoprene), plus temperature. Short-lived radicals (e.g., OH, HO<sub>2</sub>, CH<sub>3</sub>OO) were initialized at small concentrations and quickly reached daytime values determined by the core species. The six CTM/CCMs overwrote the chemical composition of a restart file, placing each pseudo-observation in a unique grid cell according to its latitude, longitude, and pressure. If another parcel is already in that cell, then it is shifted east–west or north–south to a neighboring model cell. For coarse-resolution models, multiple restart files and A runs were used to avoid large location shifts. CTM/CCMs usually have a locked in 24 h integration step starting at 00:00 UTC that is extremely difficult to modify in order to try to match the local solar time of observation, especially as it changes along aircraft flights. We tested the results with a recoded UCI CTM to start at 12:00 UTC but retain the same clouds fields over the day and found only percentage-level differences between a midnight or noon start.

These A runs averaged over cloud conditions by simulating 5 d in August at least 5 d apart. Assessment of the modeled photolysis rates and comparison with the ATom-measured *J* values is presented in Hall et al. (2018, hence H2018). All models agreed that a small fraction of chemically hot air parcels in the synthetic data set controlled most of the total reactivity. Some models had difficulty in implementing the A runs because they overwrote the specified water vapor with the modeled value, but this problem is fixed here. In both P2017 and P2018, the GISS-E2 model stood out with the most unusual chemistry patterns and sometimes illogical correlations. Efforts by a co-author to clarify the GISS results or identify errors in the implementation have not been successful. GISS results are included here for completeness in the set of three papers but are not reconciled. Overall, three models showed remarkable inter-model agreement in the three Rs with less than half of the RMSD (root-mean-square difference) as compared with the other models. UCI also tested the effect of different model years (1997 and 2015 versus reference year 2016), which varies the cloud cover and photolysis rates, and found an inter-year RMSD about half of that of the core model's RMSD. Thus, there is a fundamental uncertainty in this approach due to the inability to specify the cloud/photolysis history seen by a parcel over 24 h, but it is less than the inter-model differences among the most similar models.

## 2 Introduction

The NASA Atmospheric Tomography (ATom) mission completed a four-season deployment, each deployment flying from the Arctic to Antarctic and back, traveling south

through the middle of the Pacific Ocean, across the Southern Ocean and then north through the Atlantic Ocean, with near-constant profiling of the marine troposphere from 0.2 to 12 km altitude (see Fig. S1 in the Supplement). The DC8 was equipped with in situ instruments that documented the chemical composition and conditions at time intervals ranging from < 1 to about 100 s (Wofsy et al., 2018). ATom measured hundreds of gases and aerosols, providing information on the chemical patterns and reactivity in the vast remote ocean basins, where most of the destruction of tropospheric ozone (O<sub>3</sub>) and methane (CH<sub>4</sub>) occurs. Reactivity is defined here as in P2017 to include the production and loss of O<sub>3</sub> (P-O3 and L-O3, ppb/d) and loss of CH<sub>4</sub> (L-CH4, ppb/d). Here we report on this model-derived product that was proposed for ATom, the daily averaged reaction rates determining the production and loss of O<sub>3</sub> and the loss of CH<sub>4</sub> for 10 s averaged air parcels. We calculate these rates with 3D chemical models that include variations in clouds and photolysis and then assemble the statistical patterns describing the heterogeneity (i.e., high spatial variability) of these rates and the underlying patterns of reactive gases.

Tropospheric O<sub>3</sub> and CH<sub>4</sub> contribute to climate warming and global air pollution (Stocker et al., 2013). Their abundances in the troposphere are controlled largely by tropospheric chemical reactions. Thus, chemistry–climate assessments seeking to understand past global change and make future projections for these greenhouse gases have focused on the average tropospheric rates of production and loss and how these reactivities are distributed in large semi-hemispheric zones throughout the troposphere (Griffiths et al., 2021; Myhre et al., 2014; Naik et al., 2013; Prather et al., 2001; Stevenson et al., 2006, 2013, 2020; Voulgarakis et al., 2013; Young et al., 2013). The models used in these assessments disagree on these overall CH<sub>4</sub> and O<sub>3</sub> reactivities (a.k.a. the budgets), and resolving the cause of such differences is stymied because of the large number of processes involved and the resulting highly heterogeneous distribution of chemical species that drive the reactions. Simply put, the models use emissions, photochemistry and meteorological data to generate the distribution of key species such as nitrogen oxides (NO<sub>x</sub> = NO + NO<sub>2</sub>) and hydrogen peroxide (HOOH) (step 1) and then calculate the CH<sub>4</sub> and O<sub>3</sub> reactivities from these species (step 2). There is no single average measurement that can test the verisimilitude of the models. Stratospheric studies such as Douglass et al. (1999) have provided a quantitative basis for testing chemistry and transport and defining model errors, but few of these studies have tackled the problem of modeling the heterogeneity of tropospheric chemistry. The major model differences lie in the first step because when we specify the mix of key chemical species, most models agree on the CH<sub>4</sub> and O<sub>3</sub> chemical budgets (P2018). The intent of ATom was to collect an atmospheric sampling of all the key species and the statistics defining their spatial variability and thus that of the reactivities of CH<sub>4</sub> and O<sub>3</sub>.

Many studies have explored the ability of chemistry–transport models (CTMs) to resolve finer scales such as pollution layers (Eastham and Jacob, 2017; Rastigejev et al., 2010; Tie et al., 2010; Young et al., 2018; Zhuang et al., 2018), but these have not had the chemical observations (statistics) to evaluate model performance. In a great use of chemical statistics, Yu et al. (2016) used 60 s data ( $\sim 12$  km) from the SEAC<sup>4</sup>RS aircraft mission to compare cumulative probability densities (PDs) of  $\text{NO}_x$ ,  $\text{O}_3$ , HCHO and isoprene over the Southeast US with the GEOS-Chem CTM run at different resolutions. They identified clear biases at the high and low ends of the distribution, providing a new test of models based on the statistics rather than mean values. Heald et al. (2011) gathered high-resolution profiling of organic and sulfate aerosols from 17 aircraft missions and calculated statistics (mean, median, quartiles) but only compared with the modeled means. The HIPPER Pole-to-Pole Observations (HIPPO) aircraft mission (Wofsy, 2011) was a precursor to ATom with regular profiling of the mid-Pacific including high-frequency 10 s sampling that identified the small scales of variability throughout the troposphere. HIPPO measurements were limited in species, lacking  $\text{O}_3$ ,  $\text{NO}_x$  and many of the core species needed for reactivity calculations. ATom, with a full suite of reactive species and profiling through the Atlantic basin, provides a wealth of chemical statistics that challenge the global chemistry models.

Our task here is the assembly of the modeling data stream (MDS), which provides flight-wise continuous 10 s data (air parcels) for the key reactive species. The MDS is based on direct observations and interpolation methods to fill gaps as documented in the Supplement. Using the MDS, we have six chemical models calculating the 24 h reactivities, producing a reactivity data stream (RDS) using protocols noted in the Prologue (P2017) and described further in Sect. 2. There, we describe the updated modeling protocol RDS\* necessary to address measurement noise in key species that can be very short-lived. In Sect. 4, we examine the statistics of reactivity over the Atlantic and Pacific oceans, focusing on air parcels with high reactivity; for example, 10 % of the parcels produce 25 %–35 % of total reactivity over the oceans. We compare these ATom-1 statistics, species and reactivities with August climatologies from six global chemistry models. In one surprising result, ATom-1 shows a more reactive tropical troposphere than found in most models' climatologies associated with higher  $\text{NO}_x$  levels than in the models. Section 5 concludes that the ATom PDs based on 10 s air parcels do provide a valid chemistry metric for global models with  $1^\circ$  resolution. It also presents some examples where ATom measurements and modeling can test the chemical relationships and may address the cause of differences in the  $\text{O}_3$  and  $\text{CH}_4$  budgets currently seen across the models. With this paper we release the full ATom MDS-2 from all four deployments, along with the updated RDS\* reactivities from the UCI model.

### 3 Models and data

#### 3.1 The modeling data stream (MDS)

The ATom mission was designed to collect a multi-species, detailed chemical climatology that documents the spatial patterns of chemical heterogeneity throughout the remote troposphere. Figure S1 in the Supplement maps the 48 research flights, and the Supplement has tables summarizing each flight. We required a complete set of key species in each air parcel to initialize the models that calculate the  $\text{CH}_4$  and  $\text{O}_3$  reactivities. We choose the key reactive species ( $\text{H}_2\text{O}$ ,  $\text{O}_3$ , CO,  $\text{CH}_4$ ,  $\text{NO}_x$ , PSSNO<sub>x</sub> (photostationary state  $\text{NO}_x$ ),  $\text{HNO}_3$ ,  $\text{HNO}_4$ , PAN,  $\text{CH}_2\text{O}$ ,  $\text{H}_2\text{O}_2$ ,  $\text{CH}_3\text{OOH}$ , acetone, acetaldehyde,  $\text{C}_2\text{H}_6$ ,  $\text{C}_3\text{H}_8$ , *i*- $\text{C}_4\text{H}_{10}$ , *n*- $\text{C}_4\text{H}_{10}$ , alkanes,  $\text{C}_2\text{H}_4$ , alkenes,  $\text{C}_2\text{H}_2$ ,  $\text{C}_5\text{H}_8$ , benzene, toluene, xylene,  $\text{CH}_3\text{ONO}_2$ ,  $\text{C}_2\text{H}_5\text{ONO}_2$ ,  $\text{RONO}_2$ ,  $\text{CH}_3\text{OH}$ ) directly from the ATom measurements and then add corollary species or other observational data indicative of industrial or biomass burning pollution or atmospheric processing (HCN,  $\text{CH}_3\text{CN}$ ,  $\text{SF}_6$ , relative humidity, aerosol surface area (four modes) and cloud indicator). We choose 10 s averages for our air parcels as a compromise and because the 10 s merged data are a standard product (Wofsy et al., 2018). A few instruments measure at 1 s intervals, but the variability at this scale is not that different from 10 s averages (Fig. S2). Most of the key species are reported as 10 s values, with some being averaged or sampled at 30 s or longer such as  $\sim 90$  s for some flask measurements.

Throughout ATom, gaps occur in individual species on a range of timescales due to calibration cycles, sampling rates or instrument malfunction. The generation of the MDS uses a range of methods to fill these gaps and assigns a flag index to each species and data point to allow users to identify primary measurements and methods used for gap-filling. Where two instruments measure the same species, the MDS selects a primary measurement and identifies which instrument was used with a flag. The methodology and species-specific information on how the current MDS version 2 (MDS-2) is constructed, plus statistics on the 48 research flights and the 146 494 10 s air parcels in MDS-2, are given in the Supplement.

Over the course of this study, several MDS versions were developed and tested, including model-derived RDSs from these versions, some of which are used in this paper. In early ATom science team meetings, there was concern about the accuracy of  $\text{NO}_2$  direct measurements when at very low concentrations. A group prepared an estimate for  $\text{NO}_x$  using the  $\text{NO}$  and  $\text{O}_3$  measurements to calculate a photostationary value for  $\text{NO}_2$  and thus  $\text{NO}_x$ . This PSS- $\text{NO}_x$  became the primary  $\text{NO}_x$  source in version 0 (i.e., MDS-0). The numbering of versions initially followed the notation of revisions in the mission data archive (MDS\_R0, MDS\_R1, ...), but this was restrictive, and we adopted the simpler notation here but still beginning with version 0. With MDS-0, we chose to gap-fill using correlations with CO to estimate the variability

of the missing measurement over the gap. The science team then rejected PSS-NO<sub>x</sub> as a proxy, and we reverted to the observed NO + NO<sub>2</sub> for MDS-1, resulting in increased NO<sub>x</sub> and reactivities (RDS-1). MDS-1 NO<sub>x</sub> values are 25 % larger on average than MDS-0 values (unweighted mean of 66 vs. 52 ppt), and this affects P-O3 most and L-CH4 least. We then estimated errors in the gap-filling and found that CO had little skill as a proxy for most other species. With MDS-2, we optimized and tested the treatments of gap-filling and lower limit of detection, along with other quality controls. MDS-2 is fully documented in the Supplement.

### 3.2 The reactivity data stream (RDS)

The concept of using an MDS to initialize 3D global chemistry models and calculate an RDS was developed in the pre-ATom methodology papers (P2017; P2018). In this paper, we use the original six models for their August chemical statistics, and we use five of them plus a box model to calculate the reactivities; see Table 1. The RDS is really a protocol applied to the MDS. It is introduced in the Prologue, and the details can be found in P2018. A model grid cell is initialized with all the core reactive species needed for a regular chemistry simulation. The model is then integrated over 24 h without transport or mixing, without scavenging and without emissions. Each global model uses its own varying cloud fields for the period to calculate photolysis rates, but the FOAM box model simply takes the instant *J* values as measured on the flight and applies a diurnal scaling. We can initialize with the core species and let the radicals (OH, HO<sub>2</sub>, RO<sub>2</sub>) come into photochemical balance. The 24 h integration is not overly sensitive to the start time of the integration, and thus models do not have to synchronize with the local time of observation (see P2018's Fig. S8 and Table S8).

The initial RDS came from MDS-0 and six of the models in Table 1. This paper was nearly complete when we identified the problem with PSS-NO<sub>x</sub>. We had gathered enough information on how models agree, or disagree, with RDS-0 and thus chose to assess MDS-1 with two of the models that closely agreed (GMI and UCI). The two models were very close in RDS-0 and also in RDS-1. We then found the problems with the CO proxy and chose to use only the UCI model as a transfer standard for the change from MDS-1 to MDS-2 (i.e., RDS-1 to RDS-2). This path avoided much extra work by the modeling groups and generated the same information on cross-model differences and a robust estimate of changes from RDS-0 to RDS-2.

Statistics for the three reactivities for six models using MDS-0, 2 alternative UCI model years using MDS-0, the GMI model using MDS-1 and the UCI model using MDS-2 are given in Tables 2 and S8 for three domains: global (all points), Pacific (oceanic data from 54° S to 60° N) and Atlantic (same constraints as Pacific). UCI MDS-1 is similar to UCI MDS-2 and is not shown. The statistics try to achieve equal latitude-by-pressure sampling by weight-

ing each ATom parcel inversely according to the number of parcels in each 10° latitude by 100 hPa bin. We calculate the means and medians plus the percent of total reactivity in the top 10 % of the weighted parcels (Table 2) and also the mean reactivity of the top 10 %, percent of total reactivity in the top 50 %, 10 % and 3 % plus the mean *J* values (Table S8).

Unfortunately, while investigating sensitivities and uncertainties in the RDS for a future study, we found an inconsistency between the reported concentrations of both pernitric acid (HNO<sub>4</sub>) and peroxyacetyl nitrate (PAN) with respect to the chemical kinetics used in the models. High concentrations (attributed to instrument noise) were reported under conditions where the thermal decomposition frequency was > 0.4 per hour in the lower troposphere (> 253 K for HNO<sub>4</sub> and > 291 K for PAN). Thus, these species instantly become NO<sub>x</sub>. There is no easy fix for this, and we left the species data in the MDS as they were reported but developed a new protocol RDS\* to deal with them. Both species are allowed to decay for 24 h using their thermal decomposition rate before being put into the model. This avoids most of the fast thermal release of NO<sub>x</sub> in the 24 h of the RDS calculation but does not affect the release of NO<sub>x</sub> from photolysis or OH reactions in the upper troposphere where thermal decomposition is inconsequential. It is possible that some of the high concentrations of HNO<sub>4</sub> and PAN in the lower troposphere are real and that we are missing this large source of NO<sub>x</sub> with the RDS\* protocol, but there are no obvious sources of these species in the remote oceanic regions that would produce enough to match the thermal loss. Both this problem and its solution do not affect the initial NO<sub>x</sub>. This revised protocol (UCI2\*) is shown in Tables 2 and S8 next to the standard protocol (UCI2). The reactivities drop slightly (3 % for P-O3, 2 % for L-O3 and 0 % for L-CH4) as expected with less NO<sub>x</sub>, but the sensitivity of the reactivities to these compounds ( $\partial \ln R / \partial \ln X$ ) drops by a factor of 2 or more. We use the UCI2\* results as our best estimate of the ATom reactivities for the figures in this paper.

### 3.3 Inter-model differences

Variations in reactivities due to clouds are an irreducible source of uncertainty: predicting the cloud-driven photolysis rates that a shearing air parcel will experience over 24 h is not possible here. The protocol uses 5 separated 24 h days to average over synoptically varying cloud conditions. The standard deviation ( $\sigma$ ) of the 5 d, as a percentage of the 5 d mean, is averaged over all parcels and shown in Table S9 for the five global models. Three central models (GC, GMI, UCI) show 9 %–10 %  $\sigma$  (Js) values and similar  $\sigma$  (Rs) values as expected if the variation in *J* values is driving the reactivities. Two models (GISS, NCAR) have 12 %–17 %  $\sigma$  (Js), which might be explained by more opaque clouds, but the amplified  $\sigma$  (*R*) values (14 %–32 %) are inexplicable. This discrepancy needs to be resolved before using these two models for ATom RDS analysis.

**Table 1.** Chemistry models.

Used for	ID	Model name	Model type	Meteorology	Model grid
clim	GFDL	GFDL-AM3	CCM	NCEP (nudged)	C180 × L48
clim, MDS-0	GISS	GISS-E2.1	CCM	Daily SSTs, nudged to MERRA	2° × 2.5° × 40L
clim, MDS-0/1	GMI	GMI-CTM	CTM	MERRA	1° × 1.25° × 72L
clim, MDS-0	GC	GEOS-Chem	CTM	MERRA-2	2° × 2.5° × 72L
clim, MDS-0	NCAR	CAM4-Chem	CCM	Nudged to MERRA	0.47° × 0.625° × 52L
clim, MDS-0/1/2	UCI	UCI-CTM	CTM	ECMWF IFS Cy38r1	T159N80 × L60
MDS-0	F0AM	F0AM	box	MDS + scaled ATom Js	n/a

The descriptions of models used in the paper. The first column denotes if the model's August climatology is used ("clim") and also the MDS versions used. F0AM used chemical mechanism MCMv331 plus J-HNO<sub>4</sub> plus O<sup>1</sup>D)+CH<sub>4</sub>. For the global models, see P2017, P2017 and H2018. n/a – not applicable

**Table 2.** Reactivity statistics for the three large domains (global, Pacific, Atlantic).

Value	Region	MDS-0							MDS-1	MDS-2		
		F0AM	GC	GISS	GMI	NCAR	UCI	U15	U97	GMI1	UCI2	UCI2*
P-O <sub>3</sub> , mean, ppb/d												
	Global	1.94	1.91	2.31	1.86	1.97	2.15	2.13	2.13	2.07	2.18	2.11
	Pacific	1.91	1.95	1.94	1.92	1.92	2.13	2.08	2.10	2.06	2.33	2.26
	Atlantic	1.88	1.99	3.29	2.07	2.28	2.32	2.32	2.34	2.22	2.08	2.02
L-O <sub>3</sub> , mean, ppb/d												
	Global	1.63	1.45	1.75	1.50	1.51	1.56	1.55	1.55	1.50	1.57	1.54
	Pacific	1.60	1.48	1.74	1.51	1.44	1.54	1.50	1.52	1.48	1.53	1.50
	Atlantic	2.06	1.90	2.23	2.04	2.28	2.14	2.14	2.16	2.04	2.15	2.11
L-CH <sub>4</sub> , mean, ppb/d												
	Global	0.72	0.66	0.38	0.65	0.62	0.68	0.68	0.68	0.67	0.68	0.68
	Pacific	0.81	0.78	0.38	0.76	0.73	0.79	0.77	0.78	0.77	0.79	0.79
	Atlantic	0.77	0.74	0.49	0.77	0.80	0.80	0.80	0.81	0.79	0.79	0.79
P-O <sub>3</sub> , % of total <i>R</i> in top 10 %												
	Global	37 %	34 %	32 %	34 %	32 %	36 %	36 %	36 %	33 %	34 %	34 %
	Pacific	34 %	28 %	28 %	29 %	29 %	31 %	30 %	30 %	28 %	27 %	27 %
	Atlantic	25 %	26 %	24 %	27 %	25 %	28 %	28 %	28 %	25 %	25 %	25 %
L-O <sub>3</sub> , % of total <i>R</i> in top 10 %												
	Global	37 %	37 %	35 %	38 %	38 %	38 %	39 %	39 %	39 %	38 %	38 %
	Pacific	34 %	32 %	30 %	32 %	32 %	32 %	32 %	32 %	34 %	31 %	31 %
	Atlantic	29 %	31 %	30 %	31 %	35 %	31 %	31 %	31 %	31 %	31 %	31 %
L-CH <sub>4</sub> , % of total <i>R</i> in top 10 %												
	Global	36 %	33 %	29 %	34 %	34 %	35 %	35 %	35 %	35 %	33 %	33 %
	Pacific	33 %	29 %	26 %	30 %	30 %	30 %	30 %	30 %	31 %	27 %	27 %
	Atlantic	28 %	26 %	22 %	27 %	28 %	28 %	28 %	28 %	27 %	28 %	28 %

Global includes all ATom-1 parcels, Pacific considers all measurements over the Pacific Ocean from 54° S to 60° N and Atlantic uses parcels from 54° S to 60° N over the Atlantic basin. All parcels are weighted inversely by the number of parcels in each 10° latitude by 100 hPa bin. Results from the different MDS versions (0, 1, 2) are shown. UCI2\* uses the revised RDS\* protocol that preprocesses the MDS-2 initializations with a 24 h decay of HNO<sub>4</sub> and PAN according to their local thermal decomposition frequencies; see text. See additional statistics in Table S8.

**Table 3.** Cross-model rms differences (RMSDs as a percentage of mean) for the three reactivities.

P-O3	F0AM	GC	GISS	GMI	NCAR	UCI
F0AM		48 %	95 %	45 %	55 %	42 %
GC	48 %		78 %	<b>26 %</b>	42 %	<b>32 %</b>
GISS	95 %	78 %		81 %	72 %	75 %
GMI	45 %	<b>26 %</b>	81 %		40 %	<b>35 %</b>
NCAR	55 %	42 %	72 %	40 %		42 %
UCI	42 %	<b>32 %</b>	75 %	<b>35 %</b>	42 %	(10 %)
L-O3						
F0AM		40 %	44 %	43 %	76 %	38 %
GC	40 %		33 %	<b>25 %</b>	60 %	<b>24 %</b>
GISS	44 %	33 %		36 %	66 %	30 %
GMI	43 %	<b>25 %</b>	36 %		62 %	<b>28 %</b>
NCAR	76 %	60 %	66 %	62 %		60 %
UCI	38 %	<b>24 %</b>	30 %	<b>28 %</b>	60 %	(11 %)
L-CH4						
F0AM		47 %	136 %	48 %	82 %	45 %
GC	47 %		111 %	<b>20 %</b>	60 %	27 %
GISS	136 %	111 %		114 %	110 %	121 %
GMI	48 %	<b>20 %</b>	114 %		57 %	<b>30 %</b>
NCAR	82 %	60 %	110 %	57 %		68 %
UCI	45 %	<b>27 %</b>	121 %	<b>30 %</b>	68 %	(14 %)

Matrices are symmetric. Calculated with the 31 376 MDS-0 unweighted parcels using the standard RDS protocol. F0AM lacks 5510 of these parcels because there are no reported  $J$  values. UCI shows RMSD between years 2016 (default) and 1997 as the value in parentheses on diagonal. The unweighted mean  $R$  values from three core models (GC, GMI, UCI) are P-O3 = 1.97, L-O3 = 1.50 and L-CH4 = 0.66; all are in units of ppb/d. The three core-model RMSDs are shown in bold.

Inter-model differences are shown in the parcel-by-parcel root-mean-square (rms) differences for RDS-0 in Table 3. Even when models adopt standard kinetic rates and cross sections (i.e., Burkholder et al., 2015), the number of species and chemical mechanisms included, as well as the treatment of families of similar species or intermediate short-lived reaction products, varies across models. For example, UCI considers about 32 reactive gases, whereas GC and GMI have over 100, and F0AM has more than 600. The other major difference across models is photolysis, with models having different cloud data and different methods for calculating photolysis rates in cloudy atmospheres (H2018). The three central models (GC, GMI, UCI) in terms of their 5 d variability (Table S9) are also most closely alike in these statistics, with rms = 20 %–30 % for L-CH4 up to 26 %–35 % for P-O3. These rms values appear to be about as close as any two models can get. The intra-model rms for different years (UCI 2016 versus 1997) is 10 %–13 % and shows that we are seeing basic differences in the chemical models across GC, GMI and UCI. F0AM is the closest to the central models, but it will inherently have a larger rms because it is a 1 d calculation and not a 5 d average. NCAR's rms is consistently higher and likely related to what is seen in the 5 d  $\sigma$  values in Table S9. GISS is clearly different from all the others (L-CH4 MS > 100 %, while L-O3 rms < 66 %).

## 4 Results

Our analysis of the reactivities uses the six-model RDS-0 results to examine the consistency in calculating the Rs across models. Thereafter, we rely on the similar results from the three central models (GC, GMI, UCI) to justify use of UCI RDS\*-2 as our best estimate for ATom reactivities. The uncertainty in this estimate can be approximated by the inter-model spread of the central models as discussed above. When evaluating the model's climatology for chemical species, we use MDS-2. A summary of the key data files used here, as well as their sources and contents, is given in Table 4.

### 4.1 Probability densities of the reactivities

The reactivities for three large domains (global, Pacific, Atlantic) from the six-model RDS-0 are summarized in Tables 2 and S8. Sorted PDs for the three Rs and Pacific and Atlantic Ocean basins are plotted in Fig. 1 and show the importance of the most reactive “hot” parcels with deeply convex curves and the sharp upturn in  $R$  values above 0.9 cumulative weight (top 10 %). Both basins show a similar emphasis on the most reactive hot parcels: 80 %–90 % of total  $R$  is in the top 50 % of the parcels, 25 %–35 % is in the top 10 % and about 10 %–14 % is in the top 3 %. The corollary is that the bottom 50 % parcels control only 10 %–20 % of the total reactivity, which is why the median is less than mean (except for P-O3 in the Atlantic). Each  $R$  value and each ocean has a unique shape; for example L-O3 in the Atlantic is almost two straight lines breaking at the 50th percentile. In Fig. 1 the agreement across all models (except GISS) is clear, indicating that the conclusion in P2018 (i.e., that most global chemistry models agree on the O<sub>3</sub> and CH<sub>4</sub> budgets if given the chemical composition) also holds for the ATom-measured chemical composition. Comparing the dashed brown (UCI, RDS-0) and black (UCIP, RDS\*-2) lines, we find that the shift to observed NO<sub>x</sub> and new HNO<sub>4</sub>+PAN protocol has introduced noticeable changes only for P-O3: increasing reactivities overall in the Pacific while decreasing them slightly in the Atlantic. From Table 2, these changes primarily affected mean P-O3 and were due primarily to the shift from MDS-0 to MDS-2 and secondarily to the RDS\* protocol, which reduced both P-O3 and L-O3 in both basins. We conclude that accurate modeling of chemical composition of the 80th and greater percentiles is important but that modest errors in the lowest 50th percentile are inconsequential; effectively, some parcels matter more than others (P2017).

How well does this ATom analysis work as a model intercomparison project? Overall, we find that most models give similar results when presented with the ATom-1 MDS. The broad agreement of the cumulative reactive PDs across a range of model formulations using differing levels of chemical complexity shows this approach is robust. The different protocols for calculating reactivities as well as the uncertainty in cloud fields appear to have a small impact on the



**Table 4.** ATom data files used here.

Primary aircraft data	Formatting and content	Comments
(a) Mor.all.at1234.2020-05-27.tbl (b) Mor.WAS.all.at1234.2020-05-27.tbl (c) Mor.TOGA.all.at1234.2020-05-27.tbl All from Wofsy et al. (2018).	(a) 149 133 records $\times$ 675 csv columns, 10 s merges of flight data plus chemistry & environmental measurements (b) 6991 records $\times$ 729 csv columns, 30–120 s intervals to fill flasks (c) 12 168 records $\times$ 727 csv columns, 35 s intervals of instrument	Core source of ATom measurements. irregular and difficult formatting; extremely long ascii records; large negative integers or “NA” for some non-data.
Modeling data stream (MDS-2)		
(a) MDS_DC8_20160729_R3.ict (b) MDS_DC8_20170126_R4.ict (c) MDS_DC8_20170928_R4.ict (d) MDS_DC8_20180424_R4.ict (e) ATom_MDS.nc Derived here.	(a) ATom-1: 32 383 records $\times$ 87 csv columns, 10 s intervals of chemical & other data, plus flags to indicate gap-filling (b) ATom-2: 33 424 records $\times$ 87 csv columns (c) ATom-3: 40 176 records $\times$ 87 csv columns (d) ATom-4: 40 511 records $\times$ 87 csv columns (e) ATom MDS-2: all data in netcdf	Regular formatting; all data gap-filled; NaNs only for flight 46; for use in modeling of the chemistry and related statistics from the ATom 10 s data.
Reactivity data stream (RDS*-2)		
(a) RDS_DC8_20160729_R1.ict (b) RDS_DC8_20170126_R1.ict (c) RDS_DC8_20170928_R1.ict (d) RDS_DC8_20180424_R1.ict (e) ATom_RDS.nc Derived here.	(a) ATom-1: 32 383 records $\times$ 16 csv columns, 10 s intervals of flight data, modeled reactivities & $J$ values plus 5 d SD (b) ATom-2: 33 424 records $\times$ 16 csv columns (c) ATom-3: 40 176 records $\times$ 16 csv columns (d) ATom-4: 40 511 records $\times$ 16 csv columns (e) ATom RDS*-2: all data in netcdf	Results from UCI CTM only, using RDS* protocol and MDS-2; NaNs only for flight 46; for use analyzing the reactivities from the ATom 10 s data.

shape of the cumulative PDs but are informative regarding the minimum structural uncertainty in estimating the 24 h reactivity of a well-measured air parcel.

#### 4.2 Spatial heterogeneity of tropospheric chemistry

A critical unknown for tropospheric chemistry modeling is what resolution is needed to correctly calculate the budgets of key gases. A similar question was addressed in Yu et al. (2016) for the isoprene oxidation pathways using a model with variable resolution (500, 250 and 30 km) compared to aircraft measurements; see also ship plume chemistry in Charlton-Perez et al. (2009). ATom’s 10 s air parcels measure 2 km (horizontal) by 80 m (vertical) during most profiles. There are obviously some chemical structures below the 10 s air parcels we use here. Only some ATom measurements are archived at 1 Hz, and we examine a test case using 1 s data for O<sub>3</sub> and H<sub>2</sub>O for a mid-ocean descent between Anchorage and Kona in Fig. S2a in the Supplement. Some of the 1 s (200 m by 8 m) variability is clearly lost with 10 s averaging, but 10 s averaging preserves most of the variability. Lines in Fig. S2 demark 400 m in altitude, and most of the variability appears to occur on this larger, model-resolved scale. Figure S2b shows the 10 s reactivities during that descent and also indicates that much of the variability occurs at 400 m scales. A more quantitative example using all the tropical ATom reactivities is shown in comparisons with probability densities below (Fig. 5).

How important is it for the models to represent the extremes of reactivity? While the sorted reactivity curves

(Fig. 1, Tables 2 and S8) continue to steepen from the 90th to 97th percentile, the slope does not change that much. Thus we can estimate the 99th + percentile contributes < 5 % of the total reactivity. Thus, if our model misses the top 1 % of reactive air parcels (e.g., due to the inability to simulate intensely reactive thin pollution layers), then we miss at most 5 % of the total reactivity. This finding is new and encouraging, and it needs to be verified with the ATom-2, 3 and 4 data.

The spatial structures and variability of reactivity as sampled by the ATom tropic transects (central Pacific, eastern Pacific and Atlantic) are presented as nine panels in Fig. 2. Here, the UCI RDS\*-2 reactivities are averaged and plotted in 1° latitude by 200 m thick cells, comparable to some global models (e.g., GMI, NCAR, UCI). We separate the eastern Pacific (121° W, research flight (RF) 1) from the central Pacific (RFs 3, 4 and 5) because we are looking for contiguous latitude-by-pressure structures.

In the central Pacific (row 1), highly reactive (hot) P-O<sub>3</sub> parcels (> 6 ppb/d) occur in larger, connected air masses at latitudes 20–22° N and pressure altitudes 2–3 km and in more scattered parcels (> 3 ppb/d) below 5 km down to 20° S. High L-O<sub>3</sub> and L-CH<sub>4</sub> coincide with this 20–22° N air mass and also with some high P-O<sub>3</sub> at lower latitudes. This pattern of overlapping extremes in all three Rs is surprising because the models’ mid-Pacific climatologies show a separation between regions of high L-O<sub>3</sub> (lower-middle troposphere) and high P-O<sub>3</sub> (upper troposphere, as seen in P2017’s Fig. 3). The obvious explanation is that the models leave most of the lightning-produced NO<sub>x</sub> in the upper troposphere. The ATom

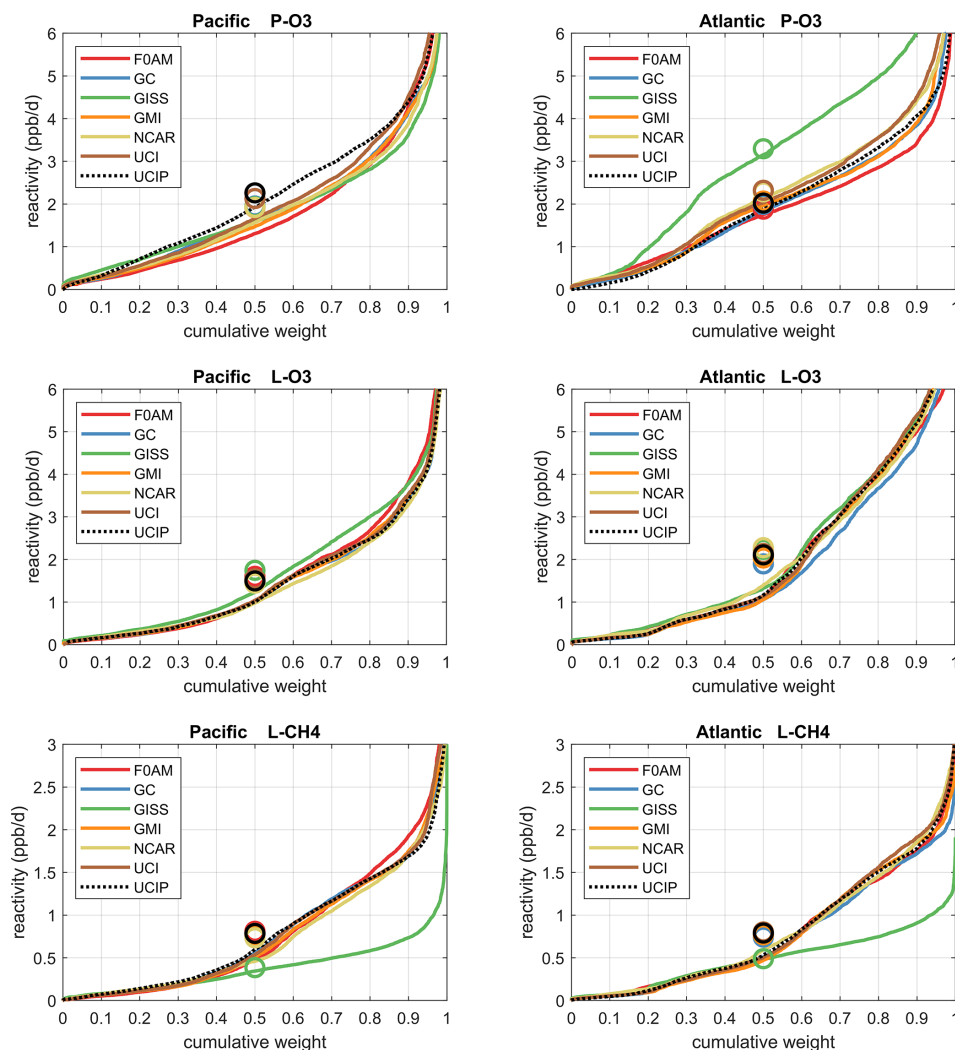


**Figure 1.** Sorted reactivities (P-O<sub>3</sub>, L-O<sub>3</sub>, L-CH<sub>4</sub>, ppb/d) for the Pacific and Atlantic domains of ATom-1. Each parcel is weighted; see text. The six modeled reactivities for MDS-0 using the standard RDS protocol are shown with colored lines, and the UCI calculation for MDS-2 using the new RDS\* protocol (HNO<sub>4</sub> and PAN damping, denoted UCIP) is shown as a dashed black line. The mean value for each model is shown with an open circle plotted at the 50th percentile. (Flipped about the axes, this is a cumulative probability density function.)

profiling seems to catch reactive regions in adjacent profiles separate by a few hundred kilometers, scales easily resolvable with 3D models.

In the eastern Pacific (row 2), the overlap of outbound and return profiles enhances the spatial sampling over the 10 h flight. The region of very large L-O<sub>3</sub> (> 5 ppb/d) is extensive, beginning at 5–6 km at 10° N and broadening to 2–8 km at 28° N. The region of L-CH<sub>4</sub> is similar, but loss at the upper altitudes of this air mass is attenuated because of the temperature dependence of L-CH<sub>4</sub> and possibly because of differing OH : HO<sub>2</sub> ratios with altitude. Large P-O<sub>3</sub> (> 6 ppb/d) occurs in some but not all of these highly reactive L-O<sub>3</sub> regions, suggesting that NO<sub>x</sub> is not as evenly distributed as HO<sub>x</sub> is. P-O<sub>3</sub> also show regions of high reactivity above 8 km that are not in the high L-O<sub>3</sub> and L-CH<sub>4</sub> regions, probably evi-

dence of convective sources of HO<sub>x</sub> and NO<sub>x</sub> but too cold and dry for the L-O<sub>3</sub> and L-CH<sub>4</sub> reactions. ATom-1 RF1 (29 July 2016) occurred during the North American Monsoon when there was easterly flow off Mexico; thus the high reactivity of this large air mass indicates that continental deep convection is a source of high reactivity for both O<sub>3</sub> and CH<sub>4</sub>.

In the Atlantic (row 3), we also see similar air masses through successive profiles, particularly in the northern tropics. The Atlantic P-O<sub>3</sub> shows high-altitude reactivity similar to the eastern Pacific. Likewise, the large values of L-O<sub>3</sub> and L-CH<sub>4</sub> match the eastern Pacific and not central Pacific. Unlike either Pacific transect, the Atlantic L-O<sub>3</sub> and L-CH<sub>4</sub> show some high reactivity below 1 km altitude. Overall, the ATom-1 profiling clearly identifies extended air masses of high L-O<sub>3</sub> and L-CH<sub>4</sub> extending over 2–5 km in altitude and

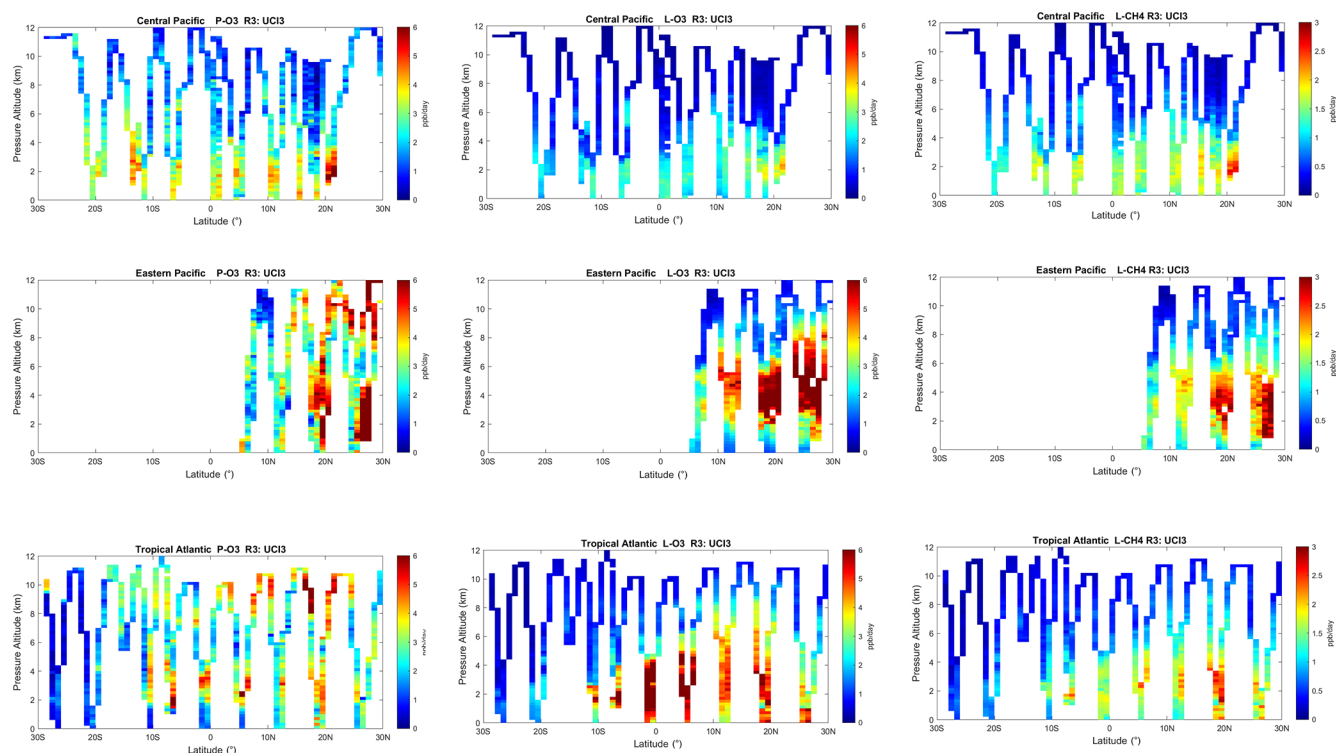


**Figure 2.** Curtain plots for P-O3 (0–6 ppb/d), L-O3 (0–6 ppb/d) and L-CH4 (0–3 ppb/d) showing the profiling of ATom-1 flights in the central Pacific (RF 3, 4 and 5), eastern Pacific (RF 1) and Atlantic (RF 7, 8 and 9). Reactivities are calculated with the UCI model R3 using MDS-2 and the new RDS\* protocol (UCI RDS\*-2). The 10 s air parcels are averaged into 1° latitude and 200 m altitude bins.

10° of latitude. The high P-O3 regions tend to be much more heterogeneous with greatly reduced spatial extent, likely of recent convective origin as for the eastern Pacific.

Overall, the extensive ATom profiling identifies a heterogeneous mix of chemical composition in the tropical Atlantic and Pacific, with a large range of reactivities. What is important for those trying to model tropospheric chemistry is that the spatial scales of variability seen in Fig. 2 are within the capability of modern global models.

### 4.3 Testing model climatologies

The ATom data set provides a unique opportunity to test CTMs and CCMs in a climatological sense. In this section, we compare ATom-1 data and the six models' chemical statistics for mid-August used in P2017. The ATom profiles cannot be easily compared point by point with CCMs, and we use statistical measures of the three reactivities in the three tropical basins: mean profiles in Fig. 3 and PDs in Fig. 5.

#### 4.3.1 Profiles

For P-O3 profiles (top row, Fig. 3), the discrepancy between models and measurements is stark. The models (less GISS) present a consistent picture of one world, while the ATom profiles describe an entirely different world. In the central Pa-

cific at 8–12 km, the ATom-1 results tend to agree with models, showing ozone production of about 1 ppb/d. Below 8 km, ATom's P-O3 increases to a peak of 4 ppb/d at 2 km, while the models' P-O3 stays constant down to 4 km and then decrease to about 0.5 ppb/d below 2 km. This pattern indicates that in the middle of the Pacific, the  $\text{NO}_x + \text{HO}_x$  combination that produces ozone is suppressed throughout the lower troposphere in all the models. In the eastern Pacific and Atlantic, both models' and ATom reactivities indicate that P-O3 is greatly enhanced above 6 km as compared to the central Pacific, but below 6 km ATom P-O3 is much larger than that of the models', by a factor of 2. In the upper troposphere, the agreement indicates that both models and ATom find the influence of deep continental convection bringing reactive  $\text{NO}_x + \text{HO}_x$  air masses to the nearby oceanic regions but not to the central Pacific. The difference below 5 km in all three regions implies a consistent bias across the models in some combination of  $\text{HO}_x$  sources and/or the vertical redistribution of lightning  $\text{NO}_x$ . This difference is unlikely to be a sampling bias in ATom-1, given it occurs in all three regions.

For L-O3 (middle row), the agreement in the central Pacific is very good throughout the 0–12 km range; i.e., ATom looks just like one of the models (except GISS). Moving to the eastern Pacific and Atlantic, both models and ATom show increased reactivity, consistent with continental convective outflow. The large ATom reactivity in the eastern Pa-

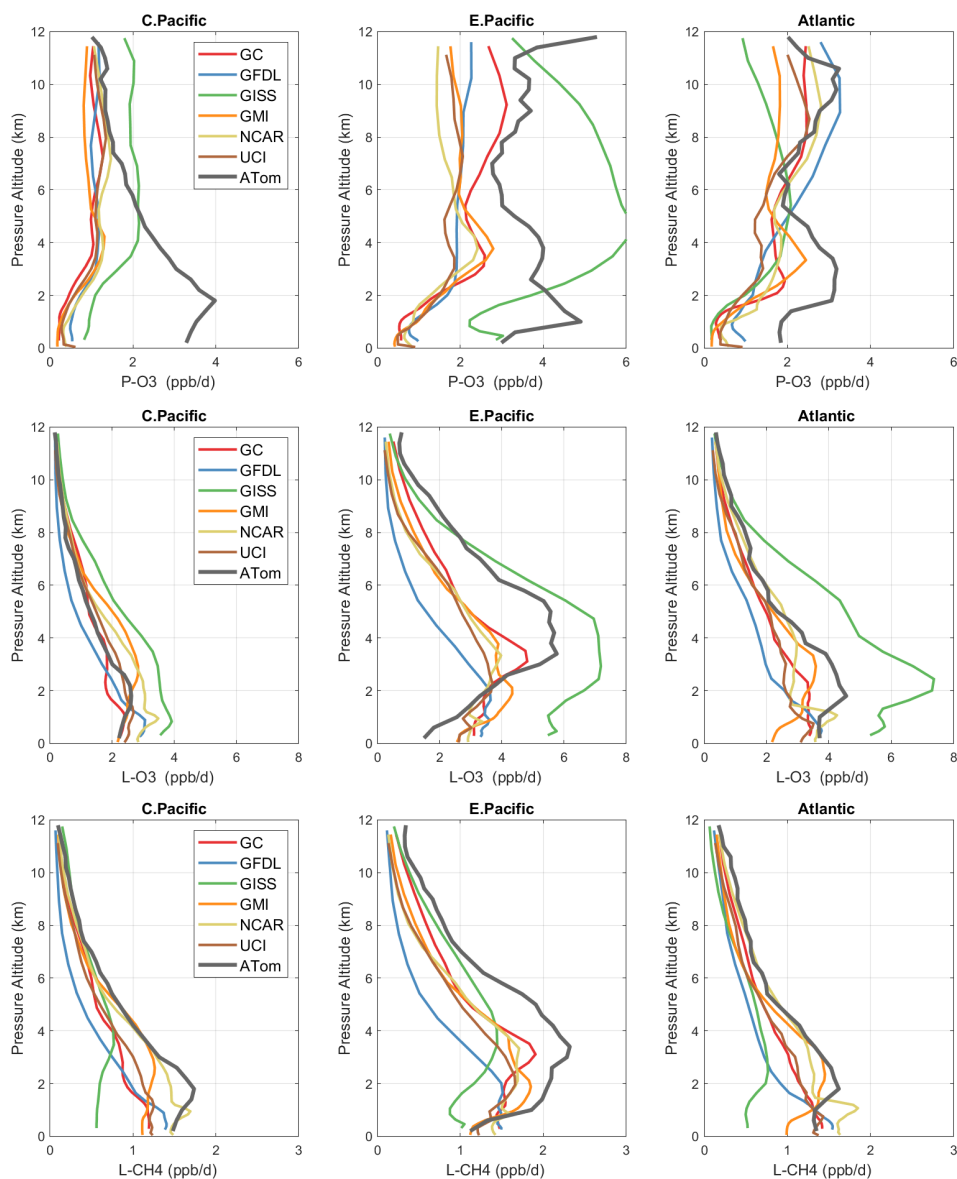


**Figure 3.** Mean profiles of reactivity (rows: P-O3, L-O3, L-CH4 in ppb/d) in three domains (columns: C. Pacific, 30° S–30° N by 180–210° E; E. Pacific, 0–30° N by 230–250° E; Atlantic, 30° S–30° N by 326–343° E). Air parcels are cosine(latitude)-weighted. ATom-1 (gray) results are from Fig. 2, while model results are taken from the August climatologies in Prather et al. (2017).

cific (3–8 km) is clear in Fig. 2 and likely due to easterly mid-tropospheric flow from convection over Mexico at that specific time (29 July 2016). Similarly, the ATom reactivity at a low level (1–3 km) in the Atlantic is associated with biomass burning in Africa and was measured in other trace species. Thus, in terms of L-O3, the ATom–model differences may be due to specific meteorological conditions, and this could be tested with CTMs using 2016 meteorology and wildfires.

For L-CH4 (bottom row), the ATom–model pattern is similar to L-O3, but higher ATom reactivity occurs at lower altitudes. Overall, the ATom L-CH4 is slightly greater than the modeled L-CH4. L-O3 is dominated by O(1D) and HO<sub>2</sub> loss,

while L-CH4 is limited to OH loss. Overall, there is clear evidence that the Atlantic and Pacific have very different chemical mixtures controlling the reactivities and that convection over land (monsoon or biomass burning) creates air masses that are still highly reactive a day or so later.

#### 4.3.2 Key species

The deficit in modeled P-O3 points to a NO<sub>x</sub> deficiency in the models, and this becomes obvious in the comparison of the PD histograms for NO<sub>x</sub> shown in Fig. 4. In the central Pacific over 0–12 km (first row), ATom has a reduced frequency of parcels with 2–20 ppt and corresponding increase

in parcels with 20–80 ppt. This discrepancy is amplified in the lower troposphere, 0–4 km (second row). In the middle of the Pacific, our chemistry models are missing a large source of lower tropospheric  $\text{NO}_x$ . The obvious source of oceanic  $\text{NO}_x$  is lightning since oceanic sources of organonitrates or other nitrate species measured on ATom could not supply this amount. The ATom statistics indicate a lightning source must be vertically mixed. In the eastern Pacific, the ATom 0–4 km troposphere appears again to have large amounts of air with 20–50 ppt, while the full troposphere more closely matches the models, except for the large occurrence of air with 100–300 ppt  $\text{NO}_x$ . These high- $\text{NO}_x$  upper troposphere regions are probably direct outflow from very deep convection with lightning in the monsoon regions over Mexico at this time. In the Atlantic, the models'  $\text{NO}_x$  shows too frequent occurrence of low  $\text{NO}_x$  ( $< 10$  ppt) and thus underestimates the 10–100 ppt levels at all altitudes. ATom has a strong peak occurrence about 80–120 ppt in the upper troposphere, and, like the eastern Pacific, this is probably due to lightning  $\text{NO}_x$  from deep convection over land (Africa or South America). Overall, the models appear to be missing significant  $\text{NO}_x$  sources throughout the tropics, especially below 4 km.

In Fig. 4, we also look at the histograms for the key  $\text{HO}_x$ -related species HOOH (third row) and HCHO (fourth row). For these species, the ATom–model agreement is generally good. If anything, the models tend to have too much HOOH. ATom shows systematically large occurrences of low HOOH (50–200 ppt, especially central Pacific), indicating, perhaps, that convective or cloud scavenging of HOOH is more effective than is modeled. HCHO shows reasonable agreement in the Atlantic, but in both central and eastern Pacific, the modeled low end ( $< 40$  ppt) is simply not seen in the ATom data. Also, the models are missing a strong HCHO peak at 300 ppt in the eastern Pacific, probably convection-related. Thus, in terms of these  $\text{HO}_x$  precursors, the model climatologies appear to be at least as reactive as the ATom data.

While the ATom-1 data in Fig. 4 are limited to single transects, the model  $\text{NO}_x$  discrepancies apply across the three tropical regions, and the simple chemical statistics for these flights alone are probably enough to identify measurement–model discrepancies. For the  $\text{HO}_x$ -related species, the models match the first-order statistics from ATom. In terms of using ATom statistics as a model metric, it is encouraging that where individual models tend to deviate from their peers, they also deviate from the ATom-1 PDs.

### 4.3.3 Probability densities

Mean profiles do not reflect the heterogeneity seen in Fig. 2, and so we also examine the PDs of the tropical reactivities (Fig. 5). The model PDs (colored lines connecting open circles at the center of each bin) are calculated from the 1 d statistics for mid-August (P2017) using the model blocks shown in Fig. S1. The model grid cells are weighted by air

mass and cosine(latitude) and limited to pressures greater than 200 hPa. The ATom PDs (black lines connecting black open circles) are calculated from the 10 s data weighted by (but not averaged over) the number of points in each  $10^\circ$  latitude by 200 hPa pressure bin and then also by cosine (latitude) to compare with the models. In addition, a PD was calculated from the  $1^\circ$  by 200 m average grid-cell values in Fig. 2 (black Xs), and this is also cosine(latitude)-weighted. To check if the high reactivities in the eastern Pacific affected the whole Pacific PD, a separate PD using only central Pacific 10 s data was calculated (gray lines connecting gray open circles). The mean reactivities (ppb/d) from the models and ATom are given in the legend; note that these values disagree with some table data that are not cosine-weighted. The PD binning is shown by the open circles, and occurrences of off-scale reactivities are included in the last point.

The obvious discrepancy is with P-O3 in both Pacific and Atlantic basins. ATom data have very low occurrence of P-O3  $< 1$  ppb/d and a broad, almost uniform frequency ( $\sim 0.1$ ) extending out to 4 ppb/d. This result is consistent with the mean profile errors (Fig. 3). The match for L-CH4 is very good in both basins, although the models have a greater occurrence in the middle 0.5–1.5 ppb/d range and reduced occurrence in the higher 1.5–2.5 ppb/d range. For L-O3, the match is very good and similar to L-CH4, although the Atlantic has a high frequency of L-O3  $> 6$  ppb/d that is not seen in the models (except GISS). The extreme eastern Pacific reactivities are seen in the mean values displayed in the legend (e.g., CPac with 1.29 ppb/d L-O3 versus ATom (i.e., CPac + EPac) with 1.54 ppb/d), but the PDs (gray circles versus black circles) resemble each other more closely than any of the models.

The ability to test a model's reactivity statistics with the ATom 10 s data is not obvious, but the PDs based on  $1^\circ$  latitude by 200 m altitude cells (the black Xs) is remarkably close to the PDs based on 2 km (horizontal) by 80 m (vertical) 10 s parcels. With the coarser resolution, we see a slight shift of points from the ends of the PD to the middle as expected, but we find once again, that the loss in high-frequency, below-model grid-cell resolution is not great. Both ATom-derived PDs more closely resemble each other than any model PD. Thus, current global chemistry models with resolutions of about 100 km by 400 m should be able to capture much of the wide range of chemical heterogeneity in the atmosphere, which for the oceanic transects is, we believe, adequately resolved by the 10 s ATom measurements. Perhaps more surprising, given the different mean profiles in Fig. 3, is that the five model PDs in Fig. 5 look very much alike. This points to some significant underlying difference between our current global chemistry models and the ATom observations.

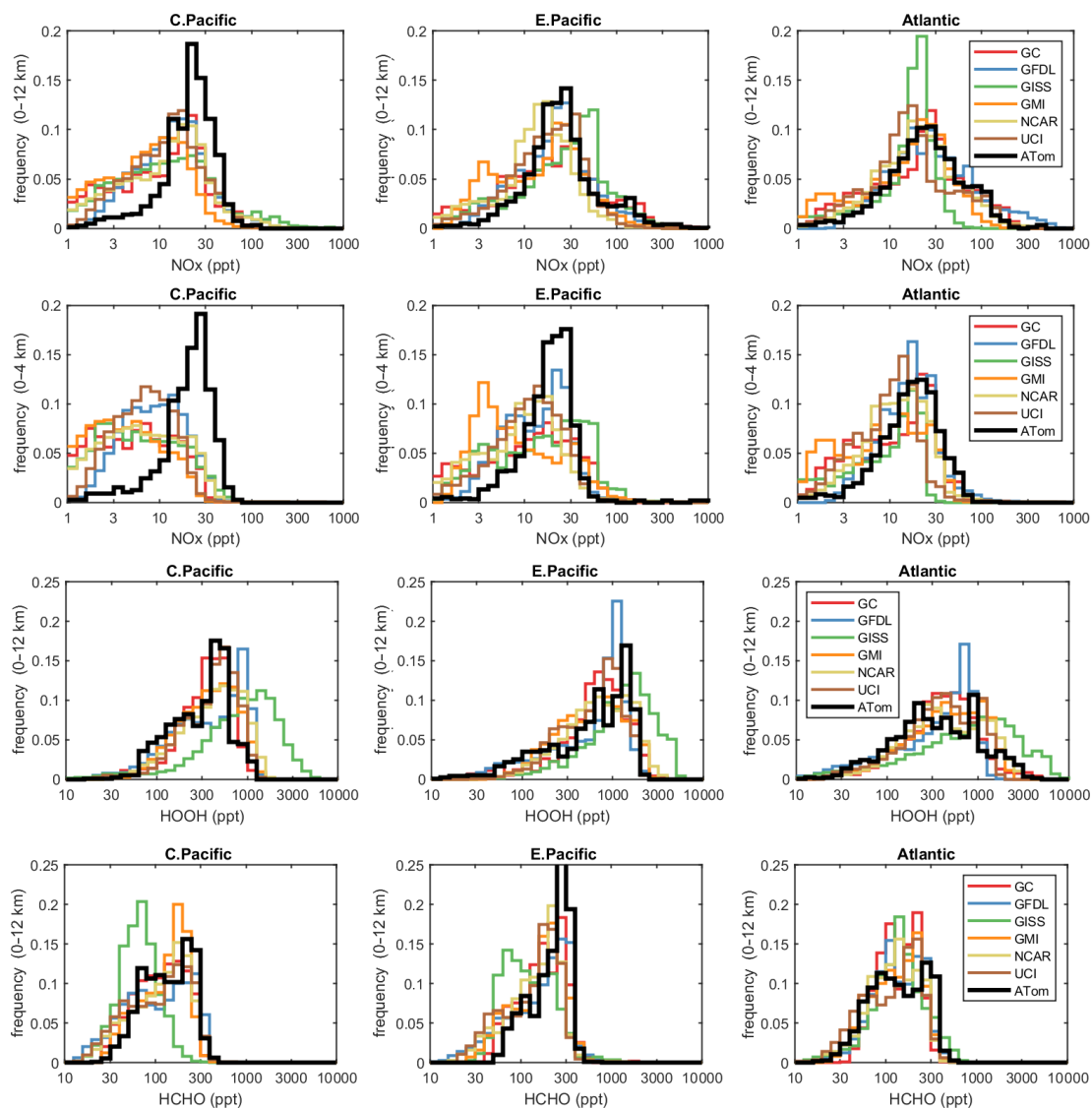


**Figure 4.** Histograms of probability densities (PDs) of  $\text{NO}_x$  (0–12 km, row 1),  $\text{NO}_x$  (0–4 km, row 2), HOOH (0–12 km, row 3) and HCHO (0–12 km, row 4) for the three tropical regions (central Pacific, eastern Pacific, Atlantic). The ATom-1 data are plotted on top of the six global chemistry models' results for a day in mid-August and sampled as described in Fig. 3.

## 5 Discussion and path forward

### 5.1 Major findings

This paper opens a door for what the community can do with the ATom measurements and the derived products. ATom's mix of key species allows us to calculate the reactivity of the air parcels and hopefully may become standard for tropospheric chemistry campaigns. We find that the reactivity of the troposphere with respect to  $\text{O}_3$  and  $\text{CH}_4$  is dominated by a fraction of the air parcels but not by so small and infrequent a fraction as to challenge the ability of current CTMs to simulate these observations and thus be used to study the oxidation budgets. In comparing ATom results with modeled

climatologies, we find a clear model error – missing  $\text{O}_3$  production over the tropical oceans' lower troposphere – and traced it to the lack of  $\text{NO}_x$  below 4 km. The occurrence of the same error over the central and eastern Pacific as well as the Atlantic Ocean makes this a robust model–measurement discrepancy.

Building our chemical statistics (PDs) from the ATom 10 s air parcels on a scale of 2 km by 80 m, we can identify the fundamental scales of spatial heterogeneity in tropospheric chemistry. Although heterogeneity occurs at the finest scales (such as seen in some 1 s observations), the majority of variability in terms of the  $\text{O}_3$  and  $\text{CH}_4$  budgets occurs across scales larger than neighboring 2 km parcels. The PDs measured in ATom can be largely captured by global models'



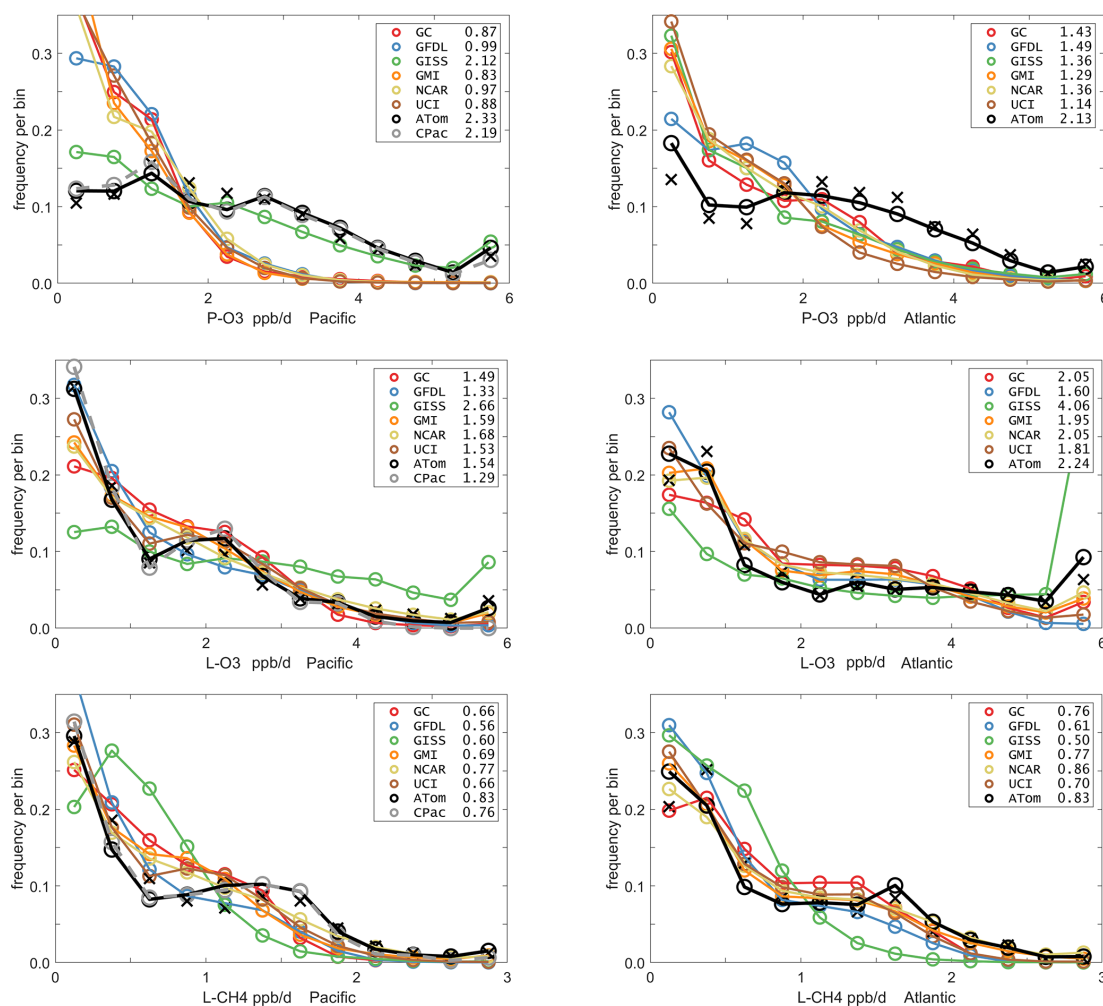


**Figure 5.** Probability densities (PDs, frequency of occurrence) for the ATom-1 three reactivities (rows: P-O3, L-O3, L-CH4 in ppb/d) and for the Pacific and Atlantic from 54° S to 60° N (columns left and right). Each air parcel is weighted as described in the text for equal frequency in large latitude–pressure bins and also by cosine(latitude). The ATom statistics are from the UCI model, using MDS-2 and revised RDS\* protocol (HNO<sub>4</sub> and PAN damping). The full Pacific results (solid black) also show just the central Pacific (dashed gray). The six models’ values for a day in mid-August are averaged over longitude for the domains shown in Fig. S1 and then cosine(latitude)-weighted. Mean values (ppb/d) are shown in the legend but are different from some tables where the cosine weighting is not applied. The PD derived from the ATom 10 s parcels binned at 1° latitude and 200 m altitude (shown for the tropics only in Fig. 2) is typical of a high-resolution global model and denoted by black Xs.

100 km by 200 m grid cells in the lower troposphere. This surprising result is evident by comparing the ATom 1D PDs – both species and reactivities – with those from the models’ climatologies (Fig. 5). These comparisons show that the modeled PDs are consistent with the innate chemical heterogeneity of the troposphere as measured by the 10 s parcels in ATom. A related conclusion for biomass burning smoke particles is found by Schill et al. (2020), where most of the smoke appears in the background rather than in pollution plumes, and therefore much of the variability occurs on synoptic scales resolved by global models (see their Fig. 1 compared with Fig. 2 here).

## 5.2 Opportunities and lessons learned

As a quick look at the opportunities provided by the ATom data, we present an example based on the Wolfe et al. (2019) study, which used the F0AM model and semi-analytical arguments to show that troposphere HCHO columns (measurable by satellite and ATom) are related to OH columns (measured by ATom) and thus to CH<sub>4</sub> loss. Figure 6 extends the Wolfe et al. study using the individual air parcels and plotting L-CH<sub>4</sub> (ppb/d) versus HCHO (ppt) for the three tropical regions where most of the CH<sub>4</sub> loss occurs. The relationship is linear, with slopes ranging from 4 to 6 per day, but the

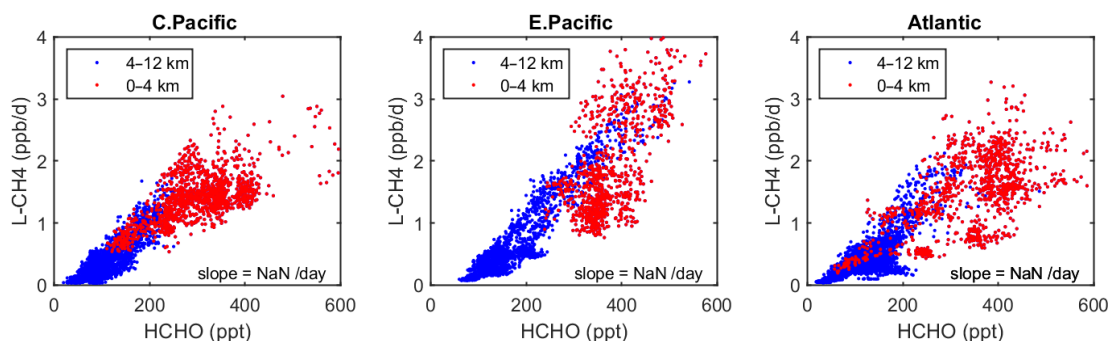


**Figure 6.** Scatterplot of L-CH<sub>4</sub> (ppb/d) versus HCHO (ppt) for ATom 1 in the three tropical regions shown in Fig. 3. The air parcels are split into the lower troposphere (0–4 km pressure altitude, red dots), where most of the reactivity lies, and the middle and upper troposphere (4–12 km, blue). A simple linear fit to all data is shown (thin black line), and the slope is given in units of 1 per day.

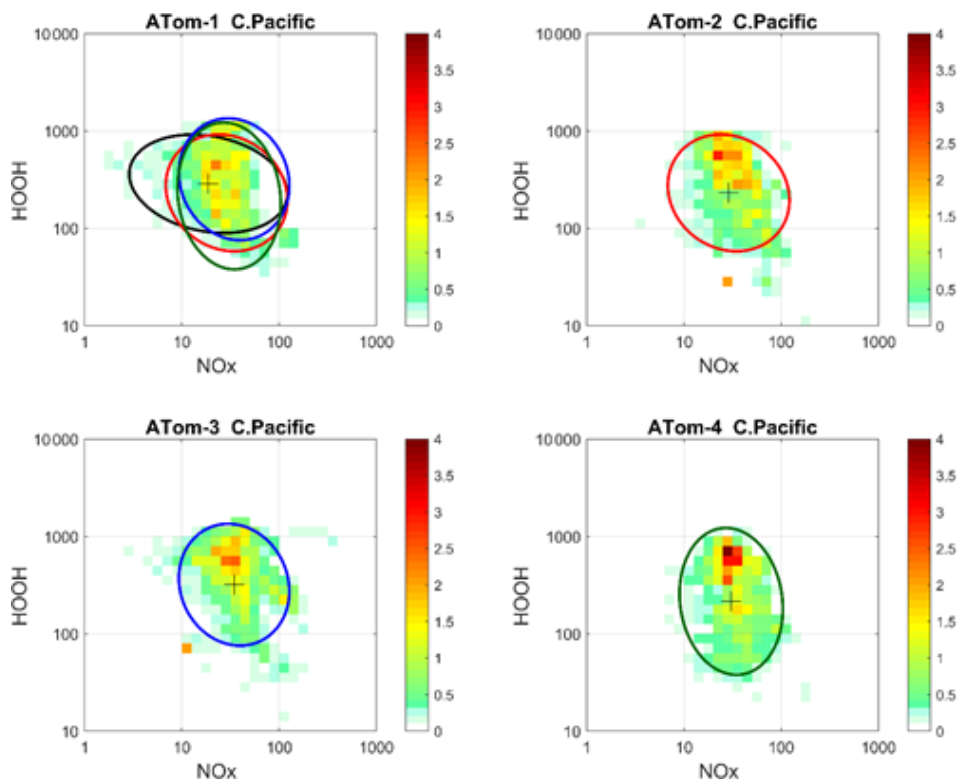


**Figure 7.** 2D frequency of occurrence (PDs in log ppt mole fraction) of HOOH vs. NO<sub>x</sub> for the tropical central Pacific for all four ATom deployments. The cross marks the mean (in log space), and the ellipse is fitted to the rotated PD having the smallest semi-minor axis. The semi-minor and semi-major axes are 2 standard deviations of PD in that direction. The ellipses from ATom-2 (red), ATom-3 (blue) and ATom-4 (dark green) are also plotted in the ATom-1 quadrant.

largest reactivities (0–4 km, 1–3 ppb/d) are not so well correlated with HCHO.

As is usual with new model intercomparison projects, we have an opportunity to identify model “features” and identify errors. In the UCI model, an error in the lumped alkane formulation (averaging alkanes C<sub>3</sub>H<sub>8</sub> and higher) did not show up in P2018, where UCI supplied all the species, but when the ATom data were used, the UCI model became an outlier. Once found, this problem was readily fixed. The divergence

of the NCAR RDS results is likely due to the implementation of the RDS protocol where CCM values overwrite the MDS values. We identified this problem in P2018 and thought it was solved, but perhaps it is not. Inclusion of the FOAM model with its extensive hydrocarbon oxidation mechanism provided an interesting contrast with the simpler chemistry in the global CCM/CTMs. For a better comparison of the chemical mechanisms, we should have FOAM use 5 d of photolysis fields from one of the CTMs. The anomalous GISS re-



sults have been examined by a co-author, but no clear causes have been identified as of this publication. The problem goes beyond just the implementation of the RDS protocol, as it shows up in the model climatology (Figs. 4 and 5, also in P2017).

Decadal-scale shifts in the budgets of O<sub>3</sub> and CH<sub>4</sub> are likely to be evident through the statistical patterns of the key species, rather than simply via average profiles. The underlying design of ATom was to collect enough data to develop such a multivariate chemical climatology. As a quick look across the four deployments, we show the joint 2D PDs on a logarithmic scale as in P2017 for HOOH versus NO<sub>x</sub> in Fig. 7. The patterns for the tropical central Pacific are quite similar for the four seasons of ATom deployments, and the fitted ellipses are almost identical for ATom 2, 3 and 4. Thus, for these species in the central Pacific, we believe that ATom provides a benchmark of the 2016–2018 chemical state, one that can be revisited with an aircraft mission in a decade to detect changes in not only chemical composition, but also reactivity.

ATom identifies which “highly reactive” spatial or chemical environments could be targeted in future campaigns for process studies or to provide a better link between satellite observations and photochemical reactivity (e.g., E. Pacific mid-troposphere in August, Fig. 2). The many corollary species measured by ATom (not directly involved in CH<sub>4</sub> and O<sub>3</sub> chemistry) can provide clues to the origin or chemical processing of these environments. We hope to engage a wider modeling community beyond the ATom science team, as in H2018, in the calculation of photochemical processes, budgets, and feedbacks based on all four ATom deployments.

**Data availability.** The MDS-2 and RDS\*-2 data for ATom 1, 2, 3 and 4 are presented here as core ATom deliverables and are now posted on the NASA ESPO ATom website (<https://espo.nasa.gov/atom/content/ATom>, Science team of the NASA Atmospheric Tomography Mission, 2021). This publication marks the public release of the reactivity calculations for ATom 2, 3 and 4, but we have not yet analyzed these data, and thus users should be aware and report any anomalous features to the lead authors via [haog2@uci.edu](mailto:haog2@uci.edu) and [mprather@uci.edu](mailto:mprather@uci.edu). Details of the ATom mission and data sets are found on the NASA mission website (<https://espo.nasa.gov/atom/content/ATom>, last access: 13 September 2021) and in the final archive at Oak Ridge National Laboratory (ORNL; [https://daac.ornl.gov/ATOM/guides/ATom\\_merge.html](https://daac.ornl.gov/ATOM/guides/ATom_merge.html), last access: 13 September 2021). The MATLAB codes and data sets used in the analysis here are posted on Dryad (<https://doi.org/10.7280/D1Q699>, Guo, 2021).

**Supplement.** The supplement related to this article is available online at: <https://doi.org/10.5194/acp-21-13729-2021-supplement>.

**Author contributions.** HG, CMF, SCW and MJP designed the research and performed the data analysis. SAS, SDS, LE, FL, JL, AMF, GC, LTM and GW contributed original atmospheric chemistry model results. GW, MK, JC, GD, JD, BCD, RC, KM, JP, TBR, CT, TFH, DB, NJB, ECA, RSH, JE, EH and FM contributed original atmospheric observations. HG, CMF and MJP wrote the paper.

**Competing interests.** The contact author has declared that neither they nor their co-authors have any competing interests.

**Disclaimer.** Publisher's note: Copernicus Publications remains neutral with regard to jurisdictional claims in published maps and institutional affiliations.

**Acknowledgements.** The authors are indebted to the entire ATom Science Team including the managers, pilots and crew, who made this mission possible. Many other scientists not on the author list enabled the measurements and model results used here. Primary funding of the preparation of this paper at UC Irvine was through NASA grants NNX15AG57A and 80NSSC21K1454.

**Financial support.** The Atmospheric Tomography Mission (ATom) was supported by the National Aeronautics and Space Administration's Earth System Science Pathfinder Venture-Class Science Investigations: Earth Venture Suborbital-2. Primary funding of the preparation of this paper at UC Irvine was through NASA (grant nos. NNX15AG57A and 80NSSC21K1454).

**Review statement.** This paper was edited by Neil Harris and reviewed by two anonymous referees.

## References

- Burkholder, J. B., Sander, S. P., Abbatt, J. P. D., Barker, J. R., Huie, R. E., Kolb, C. E., Kurylo, M. J., Orkin, V. L., Wilmouth, D. M., and Wine, P. H.: Chemical kinetics and photochemical data for use in atmospheric studies: evaluation number 18, Pasadena, CA, Jet Propulsion Laboratory, National Aeronautics and Space Administration, available at: <http://hdl.handle.net/2014/45510> (last access: 13 September 2021), 2015.
- Charlton-Perez, C. L., Evans, M. J., Marsham, J. H., and Esler, J. G.: The impact of resolution on ship plume simulations with NO<sub>x</sub> chemistry, *Atmos. Chem. Phys.*, 9, 7505–7518, <https://doi.org/10.5194/acp-9-7505-2009>, 2009.
- Douglass, A. R., Prather, M. J., Hall, T. M., Strahan, S. E., Rasch, P. J., Sparling, L. C., Coy, L., and Rodriguez, J. M.: Choosing meteorological input for the global modeling initiative assessment of high-speed aircraft, *J. Geophys. Res.-Atmos.*, 104, 27545–27564, <https://doi.org/10.1029/1999JD900827>, 1999.
- Eastham, S. D. and Jacob, D. J.: Limits on the ability of global Eulerian models to resolve intercontinental transport

- of chemical plumes, *Atmos. Chem. Phys.*, 17, 2543–2553, <https://doi.org/10.5194/acp-17-2543-2017>, 2017.
- Griffiths, P. T., Murray, L. T., Zeng, G., Shin, Y. M., Abraham, N. L., Archibald, A. T., Deushi, M., Emmons, L. K., Galbally, I. E., Hassler, B., Horowitz, L. W., Keeble, J., Liu, J., Moeni, O., Naik, V., O'Connor, F. M., Oshima, N., Tarasick, D., Tilmes, S., Turnock, S. T., Wild, O., Young, P. J., and Zanis, P.: Tropospheric ozone in CMIP6 simulations, *Atmos. Chem. Phys.*, 21, 4187–4218, <https://doi.org/10.5194/acp-21-4187-2021>, 2021.
- Guo, H.: Heterogeneity and chemical reactivity of the remote Troposphere defined by aircraft measurements, Dryad [data set], <https://doi.org/10.7280/D1Q699>, 2021.
- Hall, S. R., Ullmann, K., Prather, M. J., Flynn, C. M., Murray, L. T., Fiore, A. M., Correa, G., Strode, S. A., Steenrod, S. D., Lamarque, J.-F., Guth, J., Josse, B., Flemming, J., Huijnen, V., Abraham, N. L., and Archibald, A. T.: Cloud impacts on photochemistry: building a climatology of photolysis rates from the Atmospheric Tomography mission, *Atmos. Chem. Phys.*, 18, 16809–16828, <https://doi.org/10.5194/acp-18-16809-2018>, 2018.
- Heald, C. L., Coe, H., Jimenez, J. L., Weber, R. J., Bahreini, R., Middlebrook, A. M., Russell, L. M., Jolleys, M., Fu, T.-M., Allan, J. D., Bower, K. N., Capes, G., Crosier, J., Morgan, W. T., Robinson, N. H., Williams, P. I., Cubison, M. J., DeCarlo, P. F., and Dunlea, E. J.: Exploring the vertical profile of atmospheric organic aerosol: comparing 17 aircraft field campaigns with a global model, *Atmos. Chem. Phys.*, 11, 12673–12696, <https://doi.org/10.5194/acp-11-12673-2011>, 2011.
- Myhre, G., Shindell, D., and Pongratz, J.: Anthropogenic and Natural Radiative Forcing, in *Climate Change 2013: The Physical Science Basis*, IPCC WGI Contribution to the Fifth Assessment Report, Cambridge University Press, 659–740, <https://doi.org/10.1017/CBO9781107415324.018>, 2014.
- Naik, V., Voulgarakis, A., Fiore, A. M., Horowitz, L. W., Lamarque, J.-F., Lin, M., Prather, M. J., Young, P. J., Bergmann, D., Cameron-Smith, P. J., Cionni, I., Collins, W. J., Dalsøren, S. B., Doherty, R., Eyring, V., Faluvegi, G., Folberth, G. A., Josse, B., Lee, Y. H., MacKenzie, I. A., Nagashima, T., van Noije, T. P. C., Plummer, D. A., Righi, M., Rumbold, S. T., Skeie, R., Shindell, D. T., Stevenson, D. S., Strode, S., Sudo, K., Szopa, S., and Zeng, G.: Preindustrial to present-day changes in tropospheric hydroxyl radical and methane lifetime from the Atmospheric Chemistry and Climate Model Intercomparison Project (ACCMIP), *Atmos. Chem. Phys.*, 13, 5277–5298, <https://doi.org/10.5194/acp-13-5277-2013>, 2013.
- Prather, M. J., Ehhalt, D., Dentener, F., Derwent, R., Dlugokencky, E. J., Holland, E., Isaksen, I., Katima, J., Kirchhoff, V., Matson, P., and Midgley, P.: Chapter 4 – Atmospheric Chemistry and Greenhouse Gases, *Climate Change 2001: The Scientific Basis*, Third Assessment Report of the Intergovernmental Panel on Climate Change, 239–287, 2001.
- Prather, M. J., Zhu, X., Flynn, C. M., Strode, S. A., Rodriguez, J. M., Steenrod, S. D., Liu, J., Lamarque, J.-F., Fiore, A. M., Horowitz, L. W., Mao, J., Murray, L. T., Shindell, D. T., and Wofsy, S. C.: Global atmospheric chemistry – which air matters, *Atmos. Chem. Phys.*, 17, 9081–9102, <https://doi.org/10.5194/acp-17-9081-2017>, 2017.
- Prather, M. J., Flynn, C. M., Zhu, X., Steenrod, S. D., Strode, S. A., Fiore, A. M., Correa, G., Murray, L. T., and Lamarque, J.-F.: How well can global chemistry models calculate the reactivity of short-lived greenhouse gases in the remote troposphere, knowing the chemical composition, *Atmos. Meas. Tech.*, 11, 2653–2668, <https://doi.org/10.5194/amt-11-2653-2018>, 2018.
- Rastigejev, Y., Park, R., Brenner, M. P., and Jacob, D. J.: Resolving intercontinental pollution plumes in global models of atmospheric transport, *J. Geophys. Res.-Atmos.*, 115, D012568, <https://doi.org/10.1029/2009JD012568>, 2010.
- Schill, G. P., Froyd, K. D., Bian, H., Kupc, A., Williamson, C., Brock, C. A., Ray, E., Hornbrook, R. S., Hills, A. J., Apel, E. C., and Chin, M.: Widespread biomass burning smoke throughout the remote troposphere, *Nat. Geosci.*, 13, 422–427, <https://doi.org/10.1038/s41561-020-0586-1>, 2020.
- Science team of the NASA Atmospheric Tomography Mission: ATom [data set], available at: <https://espo.nasa.gov/atom/content/ATom>, last access: 13 September 2021.
- Stevenson, D. S., Dentener, F. J., Schultz, M. G., Ellingsen, K., Van Noije, T. P. C., Wild, O., Zeng, G., Amann, M., Atherton, C. S., Bell, N., and Bergmann, D. J.: Multi-model ensemble simulations of present-day and near-future tropospheric ozone, *J. Geophys. Res.-Atmos.*, 111, D006338, <https://doi.org/10.1029/2005JD006338>, 2006.
- Stevenson, D. S., Young, P. J., Naik, V., Lamarque, J.-F., Shindell, D. T., Voulgarakis, A., Skeie, R. B., Dalsøren, S. B., Myhre, G., Berntsen, T. K., Folberth, G. A., Rumbold, S. T., Collins, W. J., MacKenzie, I. A., Doherty, R. M., Zeng, G., van Noije, T. P. C., Strunk, A., Bergmann, D., Cameron-Smith, P., Plummer, D. A., Strode, S. A., Horowitz, L., Lee, Y. H., Szopa, S., Sudo, K., Nagashima, T., Josse, B., Cionni, I., Righi, M., Eyring, V., Conley, A., Bowman, K. W., Wild, O., and Archibald, A.: Tropospheric ozone changes, radiative forcing and attribution to emissions in the Atmospheric Chemistry and Climate Model Intercomparison Project (ACCMIP), *Atmos. Chem. Phys.*, 13, 3063–3085, <https://doi.org/10.5194/acp-13-3063-2013>, 2013.
- Stevenson, D. S., Zhao, A., Naik, V., O'Connor, F. M., Tilmes, S., Zeng, G., Murray, L. T., Collins, W. J., Griffiths, P. T., Shim, S., Horowitz, L. W., Sentman, L. T., and Emmons, L.: Trends in global tropospheric hydroxyl radical and methane lifetime since 1850 from AerChemMIP, *Atmos. Chem. Phys.*, 20, 12905–12920, <https://doi.org/10.5194/acp-20-12905-2020>, 2020.
- Stocker, T. F., Qin, D., Plattner, G. K., Tignor, M., Allen, S. K., Boschung, J., Nauels, A., Xia, Y., Bex, V., and Midgley, P. M.: Contribution of working group I to the fifth assessment report of the intergovernmental panel on climate change. Cambridge University Press, 33–115, 2013.
- Tie, X., Brasseur, G., and Ying, Z.: Impact of model resolution on chemical ozone formation in Mexico City: application of the WRF-Chem model, *Atmos. Chem. Phys.*, 10, 8983–8995, <https://doi.org/10.5194/acp-10-8983-2010>, 2010.
- Voulgarakis, A., Naik, V., Lamarque, J.-F., Shindell, D. T., Young, P. J., Prather, M. J., Wild, O., Field, R. D., Bergmann, D., Cameron-Smith, P., Cionni, I., Collins, W. J., Dalsøren, S. B., Doherty, R. M., Eyring, V., Faluvegi, G., Folberth, G. A., Horowitz, L. W., Josse, B., MacKenzie, I. A., Nagashima, T., Plummer, D. A., Righi, M., Rumbold, S. T., Stevenson, D. S., Strode, S. A., Sudo, K., Szopa, S., and Zeng, G.: Analysis of present day and future OH and methane lifetime in the ACCMIP simulations, *Atmos. Chem. Phys.*, 13, 2563–2587, <https://doi.org/10.5194/acp-13-2563-2013>, 2013.

- Wofsy, S. C.: HIAPER Pole-to-Pole Observations (HIPPO): fine-grained, global-scale measurements of climatically important atmospheric gases and aerosols, *Philos. T. R. Soc. A*, 369, 2073–2086, <https://doi.org/10.1098/rsta.2010.0313>, 2011.
- Wofsy, S. C., Afshar, S., Allen, H. M., Apel, E. C., Asher, E. C., Barletta, B., Bent, J., Bian, H., Biggs, B. C., Blake, D. R., Blake, N., Bourgeois, I., Brock, C. A., Brune, W. H., Budney, J. W., Bui, T. P., Butler, A., Campuzano-Jost, P., Chang, C.S., Chin, M., Commane, R., Correa, G., Crouse, J. D., Cullis, P. D., Daube, B.C., Day, D. A., Dean-Day, J. M., Dibb, J. E., DiGangi, J. P., Diskin, G. S., Dollner, M., Elkins, J. W., Erdesz, F., Fiore, A. M., Flynn, C. M., Froyd, K. D., Gesler, D. W., Hall, S. R., Hanisco, T. F., Hannun, R. A., Hills, A. J., Hints, E. J., Hoffman, A., Hornbrook, R. S., Huey, L. G., Hughes, S., Jimenez, J. L., Johnson, B. J., Katich, J. M., Keeling, R. F., Kim, M. J., Kupc, A., Lait, L. R., Lamarque, J.-F., Liu, J., McKain, K., McLaughlin, R. J., Meinardi, S., Miller, D. O., Montzka, S. A., Moore, F. L., Morgan, E. J., Murphy, D. M., Murray, L. T., Nault, B. A., Neuman, J. A., Newman, P. A., Nicely, J. M., Pan, X., Paplawsky, W., Peischl, J., Prather, M. J., Price, D. J., Ray, E. A., Reeves, J. M., Richardson, M., Rollins, A. W., Rosenlof, K. H., Ryerson, T. B., Scheuer, E., Schill, G. P., Schroder, J. C., Schwarz, J. P., St.Clair, J. M., Steenrod, S. D., Stephens, B. B., Strode, S. A., Sweeney, C., Tanner, D., Teng, A. P., Thames, A. B., Thompson, C. R., Ullmann, K., Veres, P. R., Vieznor, N., Wagner, N. L., Watt, A., Weber, R., Weinzierl, B., Wennberg, P. O., Williamson, C. J., Wilson, J. C., Wolfe, G. M., Woods, C. T., and Zeng L. H.: ATom: Merged Atmospheric Chemistry, Trace Gases, and Aerosols, ORNL DAAC [data set], Oak Ridge, Tennessee, USA, <https://doi.org/10.3334/ORN LDAAC/1581>, 2018.
- Wolfe, G. M., Nicely, J. M., Clair, J. M. S., Hanisco, T. F., Liao, J., Oman, L. D., Brune, W. B., Miller, D., Thames, A., Abad, G. G., and Ryerson, T. B.: Mapping hydroxyl variability throughout the global remote troposphere via synthesis of airborne and satellite formaldehyde observations, *P. Natl. Acad. Sci. USA*, 116, 11171–11180, <https://doi.org/10.1073/pnas.1821661116>, 2019.
- Young, P. J., Archibald, A. T., Bowman, K. W., Lamarque, J.-F., Naik, V., Stevenson, D. S., Tilmes, S., Voulgarakis, A., Wild, O., Bergmann, D., Cameron-Smith, P., Cionni, I., Collins, W. J., Dal-søren, S. B., Doherty, R. M., Eyring, V., Faluvegi, G., Horowitz, L. W., Josse, B., Lee, Y. H., MacKenzie, I. A., Nagashima, T., Plummer, D. A., Righi, M., Rumbold, S. T., Skeie, R. B., Shindell, D. T., Strode, S. A., Sudo, K., Szopa, S., and Zeng, G.: Pre-industrial to end 21st century projections of tropospheric ozone from the Atmospheric Chemistry and Climate Model Intercomparison Project (ACCMIP), *Atmos. Chem. Phys.*, 13, 2063–2090, <https://doi.org/10.5194/acp-13-2063-2013>, 2013.
- Young, P. J., Naik, V., Fiore, A. M., Gaudel, A., Guo, J., Lin, M. Y., Neu, J. L., Parrish, D. D., Rieder, H. E., Schnell, J. L., and Tilmes, S.: Tropospheric Ozone Assessment Report: Assessment of global-scale model performance for global and regional ozone distributions, variability, and trends, *Elementa*, 6, 10, <https://doi.org/10.1525/elementa.265>, 2018.
- Yu, K., Jacob, D. J., Fisher, J. A., Kim, P. S., Marais, E. A., Miller, C. C., Travis, K. R., Zhu, L., Yantosca, R. M., Sulprizio, M. P., Cohen, R. C., Dibb, J. E., Fried, A., Mikoviny, T., Ryerson, T. B., Wennberg, P. O., and Wisthaler, A.: Sensitivity to grid resolution in the ability of a chemical transport model to simulate observed oxidant chemistry under high-isoprene conditions, *Atmos. Chem. Phys.*, 16, 4369–4378, <https://doi.org/10.5194/acp-16-4369-2016>, 2016.
- Zhuang, J., Jacob, D. J., and Eastham, S. D.: The importance of vertical resolution in the free troposphere for modeling intercontinental plumes, *Atmos. Chem. Phys.*, 18, 6039–6055, <https://doi.org/10.5194/acp-18-6039-2018>, 2018.



*Supplement of*

## **Heterogeneity and chemical reactivity of the remote troposphere defined by aircraft measurements**

**Hao Guo et al.**

*Correspondence to:* Hao Guo (haog2@uci.edu) and Michael J. Prather (mprather@uci.edu)

The copyright of individual parts of the supplement might differ from the article licence.

## 43 **S.1. The ATom Modeling Data Stream version 2**

44  
45 The ATom mission was designed to collect a multi-species, detailed chemical climatology that  
46 documents the patterns of physical and chemical heterogeneity throughout the remote  
47 troposphere. The calculation of reactivities requires a complete set of key species in each air  
48 parcel to initialize chemistry models and then calculate the CH<sub>4</sub> and O<sub>3</sub> reactivities over a 24 hour  
49 cycle. The ATom Modeling Data Stream (MDS) provides a semi-continuous set of 10 s air  
50 parcels with a full set of values for the key chemical reactants and conditions. This  
51 supplementary methods section documents the methods used to create MDS version 2 (MDS-2).  
52 Previous MDS versions (denoted MDS...\_R0 and MDS...\_R1 in the data archive) have been  
53 distributed and used in some calculations in the main paper, but these are not fully traceable, and  
54 they are not further described here. MDS-2 has a traceable provenance as detailed here.

55  
56 ATom completed its four deployments: ATom-1 starting 20160729 (YYMMDD), ATom-2  
57 starting 20170126, ATom-3 starting 20170928, and ATom-4 starting 20180424. ATom targets  
58 the remote troposphere by sampling over the middle of the Pacific and Atlantic Ocean basins.  
59 The DC-8 aircraft performed in situ profiling of the atmosphere from 0.2 km to 12 km along each  
60 flight segment as often as possible. Each deployment lasted about 4 weeks and contained 11 to  
61 13 research flights (RF). Figure S1 maps the 48 RF, and the Table S1 summarizes each flight in  
62 terms of airports, starting date (UT), and number of 10 s parcels. We also number all the research  
63 flights consecutively as ATom flights (AF) 1 through 48. The 10 s data starts with 149,133  
64 parcels, but we collapse this to 146,494 parcels, avoiding near-airport pollution, to make MDS  
65 version 2 (MDS-2) described here. AF 46 is a short ferry flight from Kangerlussuaq, Greenland  
66 to Bangor, Maine with many instruments turned off and no profiling, thus these 1,106 parcels  
67 contain only flight data (MDS variables 1:11) and no chemical data.

68  
69 ATom sampling of the troposphere is more uniform than most aircraft missions, but still contains  
70 some biases that can be adjusted by weighting each air parcel. Due to the typical profiling  
71 sequence (level at cruising attitude for 10 min, descent for 20 min, level flight about 160 m above  
72 the sea level for 5 min, and a 20-min climb back to cruising altitude) and to the occasional  
73 requirements of weather or air traffic control, the sampling is skewed towards the uppermost  
74 troposphere ( $P < 300$  hPa) and, secondly, the marine boundary layer. For certain analyses such as  
75 probability densities (PDs) we recommend weighting each parcel inversely with the density of  
76 sampling (e.g., the number of parcels in a 10° latitude by 100 hPa pressure bin). These bins are  
77 used only for weighting each parcel and do not average the values. No parcel weights are  
78 included in MDS-2. The ATom-1 analysis selects three study domains: Global includes all  
79 parcels (32,383) weighted as above; Pacific considers all measurements (11,486) over the Pacific  
80 Ocean from 54°S to 60°N (research flights RF 1,3,4,5,6); and the Atlantic, likewise, from 54°S to  
81 60°N (RF 7, 8, 9) over the Atlantic basin (7,501). The ATom-1 flight tracks shown in Figure S1  
82 identify the Pacific and Atlantic domains with very thick lines. Also shown are the regional  
83 blocks used to calculate the model climatologies for those domains.

84  
85 We choose 10 s averages for our air parcels as a compromise to include most of the instruments,  
86 and because the 10 s merged data is a standard product (Wofsy et al., 2018). Some of our core  
87 species are measured with gas chromatographs or flask samples with longer integrations times  
88 (30-90 sec), but these can be mapped onto the 10 s parcels with loss of the higher frequency  
89 variability found in the 10 s measurements. The frequent profiling of the DC-8 gives us both  
90 vertical and horizontal scales: the vertical extent of a 10 s parcel is 50 - 110 m (55%-95% of all  
91 parcels, with <50% having near level flight) and the horizontal extent is typically 1.4 - 2.5 km  
92 (10%-90% of all parcels). A few key species have 1 Hz measurements, and, as a case study, we  
93 examine the time series of O<sub>3</sub> and H<sub>2</sub>O measured during one of the profiles of ATom-1 RF 3 in

94 Figure S2. The 1 s data is plotted along with the 10 s averages. Most of the heterogeneity  
95 including correlated variability is caught with the 10 s parcels. For all of RF 3, the root mean  
96 square error (RMSE) of the 10 s averages linearly interpolated to 1 sec is 6% for H<sub>2</sub>O and 3% for  
97 O<sub>3</sub>. The short-gap interpolation described below has an RMSE twice as large for these same  
98 species. A typical global model resolution is indicated in Figure S2 by the vertical lines spaced at  
99 500 m altitude intervals.

100  
101 The challenge in creating the MDS is the merging of multiple measurements of the same species  
102 and filling gaps in the record. MDS includes the core reactive species (H<sub>2</sub>O, O<sub>3</sub>, CO, CH<sub>4</sub>, NO<sub>x</sub>,  
103 NO<sub>x</sub>PSS, HNO<sub>3</sub>, HNO<sub>4</sub>, PAN, CH<sub>2</sub>O, H<sub>2</sub>O<sub>2</sub>, CH<sub>3</sub>OOH, acetone, acetaldehyde, C<sub>2</sub>H<sub>6</sub>, C<sub>3</sub>H<sub>8</sub>, i-  
104 C<sub>4</sub>H<sub>10</sub>, n-C<sub>4</sub>H<sub>10</sub>, alkanes, C<sub>2</sub>H<sub>4</sub>, alkenes, C<sub>2</sub>H<sub>2</sub>, C<sub>5</sub>H<sub>8</sub>, benzene, toluene, xylene, CH<sub>3</sub>ONO<sub>2</sub>,  
105 C<sub>2</sub>H<sub>5</sub>ONO<sub>2</sub>, RONO<sub>2</sub>, CH<sub>3</sub>OH) and corollary species indicative of pollution or processing (HCN,  
106 CH<sub>3</sub>CN, SF<sub>6</sub>, relative humidity, aerosol surface area (4 modes), and cloud indicator), see Table  
107 S2. Every species in each air parcel is now flagged so that the instrument is clearly identified (in  
108 the case that two instruments measure the same species) and the type of the gap filling (dependent  
109 on the length of the gap) is denoted so that the users can develop their own criteria for including,  
110 or not including, the gap-filled species. Flags 1 & 2 indicate a reported measurement from a  
111 primary (1) or secondary (2) instrument. Flag 3 means short-gap filling. Flags 4 & 6 indicate  
112 log-gap filling for tropospheric and stratospheric parcels, respectively. Flag 5 applies to missing  
113 flights with no data from that instrument(s), and these were filled by a multiple linear regression  
114 from the parallel flights. Flag 0 indicates not a number (NaN), which only occurs for AF 46.  
115 Thus, while the MDS creates a continuous stream of fully speciated 10 s air parcels, the users can  
116 sub-select, for example, only the direct measurements from the primary instrument.

### 117 118 **S.1.1. The primary ATom data sets**

119  
120 The 'Mor' data sets created by Wofsy et al. (2018) contain merges of the ATom 10 s data  
121 (Mor.all), the WAS flask data analyzed post-flight (Mor.WAS.all) and the in-flight TOGA  
122 chromatograph-mass spectrometer data (Mor.TOGA.all). These data sets are released in a gzip  
123 file with the YYYY-MM-DD of their creation. For this MDS version (2020-05-27), we use the  
124 following 3 data sets:

125 'Mor.all.at1234.2020-05-27.tbl' (653,494,900 bytes)

126 'Mor.WAS.all.at1234.2020-05-27.tbl' (49,091,169 bytes)

127 'Mor.TOGA.all.at1234.2020-05-27.tbl' (80,579,206 bytes)

128  
129 The Mor data are ASCII text files with extremely long records and difficult to read, containing a  
130 mix of comma-separated floating point, integer and character strings. For Mor.all, the 149133  
131 records contain 675 comma-separated variables (but this can change with different releases).  
132 Some of the floating point variables are longer than 20 characters due to excess precision in the  
133 scientific notation. We pre-process these with a Fortran generic read(5,\*) using the comma  
134 separation to generate character strings. The code searches the title (first) record of the Mor...tbl  
135 to identify the specific columns that we need for MDS (in this case 39 out of 675). The 39 key  
136 data from each record are rewritten in formatted form (39a40, because some floating point  
137 variables were excessively long and 39a20 was inadequate) with comma separation. All  
138 numerical values are copied verbatim, but the text 'NA' is replaced by 'NaN'. This new file can be  
139 simply imported into Matlab or more easily read by other software. Further, this approach  
140 ensures that the correct quantities are pulled from the Mor...tbl file, even if the column order  
141 changes due to addition or removal of data. The WAS and TOGA observations have separate  
142 files with the start and end times of the observed air mass, which is greater than the 10s interval in  
143 the regular file. Both WAS & TOGA Mor...data sets have a large number of data columns (729  
144 & 727) with fewer records (6,991 & 12,168, respectively).

145  
146  
147  
148  
149  
150  
151  
152  
153  
154  
155  
156  
157  
158  
159  
160  
161  
162  
163  
164  
165  
166  
167  
168  
169  
170  
171  
172  
173  
174  
175  
176  
177  
178  
179  
180  
181  
182  
183  
184  
185  
186  
187  
188  
189  
190  
191  
192  
193  
194  
195

The 3 Fortran output files are imported into Matlab (using 'Import Data') and then processed as described below. The instructions and Matlab code are included in text files containing Matlab commands: 'Pmat-Mor1.txt', 'Pmat-WAS+TOGA.txt', 'Pmat-MDS0n.txt').

### S.1.2. Preliminary processing and identifying gaps

In terms of critical flight data (time, latitude, longitude, altitude), there are no gaps in the record. UTC\_stop has a gap, but this variable is not used in the MDS (10s intervals are assumed).

The Mor.all.at1234.2020-05-27 data set of 149,133 10s parcels was sorted into deployments and research flights. The beginning and end points of each research flight (RF) along with the deployment and starting date of each flight are given in Table S1. All together there are 48 flights, but AF 46 contains only flight data. All three types of Mor data include some measurements close to the airports, which often have ground-level pollution. We remove these data by including only measurements at altitudes of 900 m or more above the takeoff/landing airport. The record collapses to 146,494 parcels, also shown in Table S1.

The list of MDS-2 variables, their MDS identifiers (all ending in \_M) and the sources in standard ATom nomenclature are given in Table S2. The flag variables (0 to 6) are also explained there. Information about each research flight is summarized in **Table S3abcd**, including the average latitude, longitude and altitude of the 10s parcels (all equally weighted here). The abcd sub-tables correspond to the 4 deployments. For each of the MDS variables 12 to 50, The % of non-NaN values with flags = 1, 2 or 3, is shown (the remaining % has flags = 4, 5 or 6). These data correspond to a primary or secondary direct measurement (1 or 2) or else short-gap interpolation (3, see text below). Missing data for an entire flight (0%) has shaded cells.

**Mor.all combined species and fixes.** The primary MDS NO<sub>x</sub> values were created by simply summing NO\_CL + NO<sub>2</sub>\_CL before any attempt to deal with the negative values. The number (27071) of NO<sub>x</sub> NaNs coincides with those of NO<sub>2</sub>\_CL. The alternative photostationary state NO<sub>x</sub> values (NO<sub>x</sub>PSS) were calculated from O<sub>3</sub>, NO and J-values and was originally proposed as a more accurate value for NO<sub>x</sub>. Subsequent analysis has shown this approach is biased, and it is included here only for ATom-1 because some early model studies used it in the MDS-0 version. A small number (22) of CH<sub>4</sub>\_QCLS values have unrealistic abundances <1000 ppb and these are converted to NaNs. The NaNs in these cases were filled using the algorithm below.

**TOGA and WAS combined species and immediate fixes.** Methyl and ethyl nitrate (WAS only) are kept separately but the 6 higher organo-nitrates are combined into RONO<sub>2</sub>; the limited TOGA organo-nitrates are not used. For both WAS and TOGA, toluene and ethylbenzene are combined into toluene, and the two forms of xylene are combined. Both forms of butane are kept, but higher alkanes are combined into 'Alkanes' for both TOGA and WAS. TOGA and WAS use -888 flags for LLOD and these are converted to 0.001 ppt because the LLOD values for these species (e.g., 3 ppt) are much higher than remote background values and setting them to the LLOD level would be misleading. TOGA's toluene has some mistaken values of 888 and 999 instead of -888 and -999 and these are corrected. All -999 values, as well as all gaps in either TOGA or WAS measurement intervals are converted to NaNs. The WAS and TOGA data have time stamps (stop minus start) much longer than the 10 sec parcels in the Mor.all data sets, and their values are mapped onto the 164,494 parcels whenever their start or stop time falls within the 10s start-stop range, else they are filled with NaNs. The WAS and TOGA instruments sample air averaged over typically 30 to 90 sec, and then have a gap before the next measurement, varying from 30 to 300 sec. The TOGA length-of-measurement is regular with the 10%-90%ile range

196 being about 35 sec and the same percentile length-of-gaps being about 85 sec. The WAS data  
197 comes from flasks filled in flight, and the time to fill a flask depends on the pressure, and the gap  
198 depends on the operator decision: the 10%-90%ile length-of-measurement is 32 to 90 sec, and  
199 the corresponding gaps are 33 to 285 sec.

200

### 201 **S.1.3. Interpolation and fill of data gaps**

202

203 The actions here are arbitrary but judicious, and every attempt was made to avoid introducing  
204 spurious data. There are a number of negative values for chemical variables that are intrinsically  
205 positive definite. Instrument reporting of a negative value is expected when the concentration is  
206 near the limit of detection or within the instrumental noise range. The MDS choice is simply to  
207 take all such values less than or equal to 0 and convert to 0.001 ppt. Since these negative values  
208 usually represent a small concentration close to the detection limit, they have little impact on the  
209 chemistry calculations using the MDS. If analyzing statistics near this range, the original Mor  
210 data sets should be used.

211

212 **Pressure and temperature.** P and T have 5 very small gaps of length ~6 (# of 10s parcels  
213 missing) plus a longer gap of length 28. All gaps occurred during smooth descent or ascent and  
214 so were filled using linear interpolation. These are denoted by  $\text{flag\_M}(:,10) = \text{flag\_M}(:,11) = 3$ .  
215 In this document we are careful to give measured species a suffix that denotes their provenance,  
216 and thus the MDS variables denoting the combined, continuous data are labeled P\_M and T\_M.

217

218 **H<sub>2</sub>O and relative humidity.** There are a number of short gaps in the record of H<sub>2</sub>O\_DLH and  
219 RHw\_DLH, and only 2 longer gaps (length = 83 and 87). One of the long gaps occurs during  
220 descent as H<sub>2</sub>O jumps from 240 to 18,000 ppm. Thus we choose a linear in the log method for all  
221 H<sub>2</sub>O gaps, while a simply linear method is used to fill RHw gaps. These are denoted by  
222  $\text{flag\_M}(:,12) = \text{flag\_M}(:,13) = 3$ . The MDS variables denoting the combined data are H2O\_M  
223 and RHw\_M.

224

225 **CO.** In our first attempts to produce a gap-filled record for chemical modeling, we sought a  
226 species with continuous measurement that could be used as a proxy for unusual or polluted air  
227 during the gaps in other species. CO was the obvious species because it is indicative of biomass  
228 burning or industrial pollution, and ATom has two well calibrated, nearly continuous  
229 measurements: CO\_NOAA and CO\_QCLS. The primary CO data are from QCLS because it has  
230 higher precision and the secondary are from NOAA which has fewer gaps. Unfortunately, after  
231 creating this gap-filled CO data and applying it as a proxy for MDS versions 0 and 1, we found  
232 that CO had little skill in filling the gaps in other species. We use this method to generate our  
233 CO\_M record for the MDS, but do not use it for other species. This processing of the CO data  
234 was done with the full 149,133-parcel dataset, and not the airport-collapsed data set. For the  
235 MDS airport-truncated data set, CO\_NOAA has 8463 gaps; and CO\_QCLS has 30,233. Most all  
236 of these gaps are short and part of the instrument cycling.

237

238 1. Modify CO\_QCLS: interpolate short gaps in the CO\_QCLS record ( $\leq 10$  parcels = 100s ~

239 1000 m vertically)

240

- 241 2. Create a continuous CO\_N record.
  - 242 a. Start with CO\_NOAA and locate all the NaN gaps.
  - 243 b. Fill gaps with modified CO\_QCLS where available and locate new NaN gaps.
  - 244 c. Average CO for 5 points on either side of gap, interpolate linearly across the gaps.
- 245 3. Smooth the CO\_N record, which is visibly noisy at 10 s with 11-point running average (~
- 246 1000 m in vertical).

245

246

- 246 a. Define CO = modified CO\_QCLS (step 1).



- 247           b. Fill the gaps in CO with CO\_N (step 3).  
248           c. Define CO flags:  
249                 1 = primary, QCLS (116,261 parcels);  
250                 2 = secondary, smoothed CO\_N (29428);  
251                 3 = modified, short-interpolated QCLS (80);  
252                 4 = interpolated CO\_N (725).  
253

254 Two samples of this CO interpolation method are shown in Figure S3. The frequency of  
255 occurrence of all flags for this new CO\_M variable, along with the other MDS chemical  
256 variables, are given in Table S4. About 99% of the CO\_M records are from direct measurements  
257 (QCLS or NOAA), and this is matched only by the H<sub>2</sub>O and O<sub>3</sub> measurements.  
258

259 **Short-gap simple interpolation for remaining species.** It was decided that the least intrusive  
260 method for filling short data gaps was to simply interpolate using only the instrument data. In  
261 MDS versions 0 and 1, CO was used as a proxy to fill these gaps, but later analysis showed little  
262 correlation with absolute CO or even the short-term variability in CO. We examined the typical  
263 size of gaps and their frequency. For the Mor.all species we selected gaps of  $\leq 13$  for short-gap  
264 interpolation; for WAS the gap frequency peaked about 10 (100 s) and we selected gaps of  $\leq 10$ ;  
265 for TOGA there was a strong peak at gap length of 7-8 (instrument cycle time) and we also  
266 selected  $\leq 10$  as the criterion. These gaps correspond to about 1000 m or less in the vertical  
267 during ascent or descent. For most Mor.all variables this adds about 10% (absolute) to the number  
268 of non-NaN parcels, but for WAS and TOGA with many smaller gaps it greatly enhances the  
269 coverage. WAS coverage goes from 28% to 41%, while TOGA jumps from 31% to 93% because  
270 most gaps are 85 sec. For all short-gap interpolation, the parcel data for that species is tagged  
271 with flag = 3.  
272

273 **Long-gap interpolation for remaining species - Troposphere.** We choose a robust and  
274 minimally intrusive method for filling gaps  $> 10$  (100 s) based upon the average tropospheric  
275 profile for that flight, using eight 100-hPa-wide bins ( $< 300$ , 300-400, 400-500, 500-600, 600-700,  
276 700-800, 800-900,  $> 900$  hPa). The gap value is replaced by the appropriate bin value. If any  
277 bins have no measured values, we use the nearest bin or average of the nearest bins. It is  
278 important not to confuse stratospheric and tropospheric air when gap filling. From our analysis, a  
279 number of key reactive species (e.g., CH<sub>2</sub>O, HOOH, NO<sub>x</sub>) show distinctly different patterns as  
280 ATom crosses into the stratosphere.  
281

282 **Long-gap interpolation - Stratosphere.** We find the most robust definition of stratospheric-like  
283 air to be based primarily on H<sub>2</sub>O rather than O<sub>3</sub>, because O<sub>3</sub> abundances  $> 200$  ppb are often seen  
284 in large, clearly tropospheric air masses with H<sub>2</sub>O  $> 50$  ppm. Based on percentiles of O<sub>3</sub> at  
285 different values of H<sub>2</sub>O (see Figure S4a) we pick  $< 30$  ppm as the criteria for being stratospheric,  
286 with the secondary requirements that O<sub>3</sub>  $> 80$  ppb and CO  $< 120$  ppb (see Figure S4b). For the  
287 stratospheric air we create mean 'profiles' in terms of 6 O<sub>3</sub> bins ( $< 200$ , 200-300, 300-400, 400-  
288 500, 500-700,  $> 700$  ppb) use this as a lookup table for gap filling. There are many fewer  
289 stratospheric parcels, and the stratosphere tends to be similar across latitudes, and so we create a  
290 single lookup tables from all research flights at all latitudes. In general, these near tropopause air  
291 parcels are cold and dry and not highly reactive; however when partitioning the chemistry model  
292 calculated reactivities between stratosphere and troposphere, these criteria may need to be re-  
293 investigated.  
294

295 As a measure of the error in this long-gap interpolation, we randomly select 10% of the air  
296 parcels from data stream before calculating the long-gap interpolation, interpolate those 10%  
297 points, and calculate the mean bias and root-mean-square error (rmse). This is repeated 10 times

298 and we show the average results in Table S5 below. We find these results acceptable, and better  
299 than the multiple linear regressions we tried. There may be a better way to do this in future  
300 versions MDS-2, perhaps with a machine-learning approach. Gaps interpolated in this way are  
301 given flag = 4 (troposphere tables) and flag = 6 (stratosphere tables).  
302

303 **Missing data for an entire flight.** For **ATom-1 RF-5**, an instrument failed and we lost all data  
304 for H2O2\_M, HNO3\_M, and HNO4\_M. This flight was from American Samoa to Christ  
305 Church. We fill these species using a multiple linear regression from the parallel flights ATom-1  
306 RF-4 and ATom-2/3/4 RF-4/5. The independent (explanatory) variables for the multiple linear  
307 regression for these missing flights are chosen to be pressure, noontime solar zenith angle and  
308 latitude (in that order). For H2O2\_M and HNO3\_M, we calculate the missing ATom-1 RF-5 data  
309 using the full set of parallel flights, but for HNO4\_M, we can use only ATom-1/2 flights (see  
310 Table S3 & S6). Data filled for missing flights are given flag = 5. For **ATom-2 RF-2**, we also  
311 lost all data for H2O2\_M, HNO3\_M, and HNO4\_M. In this case the regression is based on  
312 parallel flights ATom-2 RF-3 and ATom-1/3/4 RF-2/3 for H2O2\_M and HNO3\_M, but only  
313 ATom-2 RF-3 and ATom-1 RF-2/3 for HNO4\_M. For **ATom-3 RF-1**, we lost all data for  
314 NO<sub>x</sub>\_M. A multiple linear regression is based on parallel flights ATom-3 RF-2 and ATom-1/2/4  
315 RF-1/2. For **ATom-3/4 all**, we lost all data for HNO4\_M, and the best we can do is base the  
316 regression on all HNO4\_M measurements (not filled as noted above) from ATom-1/2. This is  
317 clearly one of the weakest gap filled here, and users should be careful if key results depend  
318 HNO4\_M values for ATom-3/4. For **ATom-4 RF-5/6/7/8/9/12/13**, we lost all data for  
319 CH3OOH\_M. A multiple linear regression approach was based on data from the preceding RF-4  
320 as well as the parallel research flights from the other 3 deployments (i.e., ATom-1/2 RF-5 to 11,  
321 ATom-3 RF-5 to 13, ATom-4 RF-4). For **ATom-4 RF-11** (AF 46), all chemical data have flag =  
322 0, value = NaN. A summary of the missing flights and species along with estimated error in our  
323 gap filling is given in Table S6.  
324

325 From the reactivity results for ATom-1 shown in this paper, the lack of ATom-3 NO<sub>x</sub>  
326 observations in the Eastern Pacific (RF 1) mean that the P-O3 statistics there (not calculated in  
327 this paper) will not be useful.  
328

#### 329 **S.1.4. Species measured by two instruments**

330  
331 Several species have redundant measurements and these are identified by the duplicate sources in  
332 Table S2. The choice of primary (flag = 1) and secondary (flag = 2) are chosen based on  
333 continuity of record or coverage of related species, or our estimate of the higher precision  
334 measurement. Primary data sources usually have a better data coverage.  
335

336 **CH<sub>4</sub>:** (1) CH<sub>4</sub>\_NOAA, (2) CH<sub>4</sub>\_QCLS. The primary has more data and does not have spurious  
337 anomalies. There is no evident bias, but some scatter, and so the NaNs in the primary record  
338 (which first has had short-gap interpolation as noted above) are simply filled with the secondary  
339 record (also with short-gap interpolation).  
340

341 **CH<sub>2</sub>O:** (1) CH<sub>2</sub>O\_ISAF, (2) CH<sub>2</sub>O\_TOGA. Formaldehyde is a key reactive species and TOGA  
342 provides a secondary record for the 2<sup>nd</sup> half of ATom-4 when ISAF failed. The overlapping data  
343 with both instruments is plotted in below (Figure S5). The mean difference in overlapping  
344 observations is very small (-1 out of a mean of 134 ppt), but the rms is larger (75 ppt). ISAF has  
345 a number of values > 1000 ppt, while TOGA has none. A linear fit gives a slope of 0.8 with R<sup>2</sup> =  
346 0.59, but a 1:1 slope has only slightly smaller R<sup>2</sup> = 0.55. We do not attempt to rescale the TOGA  
347 data in this case and just replace any NaNs remaining in the short-gap-interpolated ISAF record  
348 (particularly flights 42:48) with TOGA data (also short-gap interpolated).

349  
350 **PAN:** (1) PAN\_GTCIMS, (2) PAN\_PECD\*. The GTCIMS joined the mission at ATom-2. The  
351 overlap period shows a clear bias between the GTCIMS and PECD observations. A linear fit is  
352 clear ( $R^2 = 0.84$ ), and we rescale the secondary  $PECD^* = (PECD + 0.45)/1.18$ .  
353  
354 **C<sub>3</sub>H<sub>8</sub>:** (1) Propane\_WAS, (2) Propane\_TOGA. No obvious bias is found. A linear fit gives an  
355  $R^2 = 0.90$ , but the 1:1 line has an  $R^2 = 0.85$ , so we just use the TOGA data directly as the  
356 secondary observation.  
357  
358 **iC<sub>4</sub>H<sub>10</sub>:** (1) iButane\_WAS, (2) iButane\_TOGA. No obvious bias is found. A linear fit gives an  
359  $R^2 = 0.955$ , but the 1:1 line has an  $R^2 = 0.947$ , so we just use the TOGA data directly as the  
360 secondary observation.  
361  
362 **nC<sub>4</sub>H<sub>10</sub>:** (1) nButane\_WAS, (2) nButane\_TOGA. No obvious bias is found. A linear fit gives an  
363  $R^2 = 0.962$ , but the 1:1 line has an  $R^2 = 0.942$ , so we just use the TOGA data directly as the  
364 secondary observation.  
365  
366 **C<sub>5</sub>H<sub>8</sub>:** (1) Isoprene\_TOGA, (2) Isoprene\_WAS. No obvious bias is found. A linear fit gives an  
367  $R^2 = 0.938$ , but the 1:1 line has an  $R^2 = 0.904$ , so we just use the WAS data directly as the  
368 secondary observation.  
369  
370 **benzene:** (1) Benzene\_TOGA, (2) Benzene\_WAS. There is some systematic difference between  
371 WAS and TOGA ( $TOGA = \sim 0.75 \times WAS$ ), but the contribution of WAS to the aromatics is small  
372 (see  $flag=2$  is  $<3\%$  in **Table S4**) and so we did not scale WAS.  
373  
374 **toluene:** (1) Toluene\_TOGA + EthBenzene\_TOGA, (2) Toluene\_WAS + EthBenzene\_WAS. No  
375 obvious bias is found in spite of the large scatter. A linear fit gives an  $R^2 = 0.75$ , but the 1:1 line  
376 has an  $R^2 = 0.74$ , so we just use the TOGA data directly as the secondary observation.  
377  
378 **xylene:** (1) mpXylene\_TOGA + oXylene\_TOGA, (2) mpXylene\_WAS + oXylene\_WAS. No  
379 obvious bias is found in spite of the very large scatter. A linear fit gives an  $R^2 = 0.3$ , so we just  
380 use the WAS data directly as the secondary observation.  
381  
382 **HCN:** (1) HCN\_CIT, (2) HCN\_TOGA. The CIT observation is chosen as primary because of its  
383 more continuous, 10s record. In spite of the large scatter, a linear fit with a slope of 0.8 does not  
384 greatly reduce the variance ( $R^2 = 0.74$  vs 0.65 for 1:1), so we just use the TOGA data directly as  
385 the secondary observation.  
386  
387 **SF<sub>6</sub>:** (1) SF<sub>6</sub>\_PECD, (2) SF<sub>6</sub>\_UCATS. The scatter seems large, but the relationship is mostly  
388 1:1 with  $R^2 = 0.90$ . A linear fit gives a slope of 0.99, and so we just use the UCATS data directly  
389 as the secondary observation. Both data sets are sparse.

## 390 391 **S.2. The Reactivity Data Stream** 392

393 In this paper, we use 6 global atmospheric chemistry models for their August chemical statistics.  
394 We use 5 of these models plus a box model to calculate the Reactivity Data Stream (RDS, i.e.,  
395 chemical tendencies) for each ATom-1 MDS 10 s air parcel. The models are summarized in the  
396 main paper Table 1 and with more detail in Table S7 here. Statistics of the reactivities and J-  
397 values across models and MDS versions are shown in the main Table 2 and Tables S8abc here.  
398 Table S9 gives the standard deviation when averaging across 5 separated days in August (% of

399 mean reactivity or J-value). See the main paper for a description of the RDS protocol and its  
400 updates (RDS\* used in UCI2\*).  
401

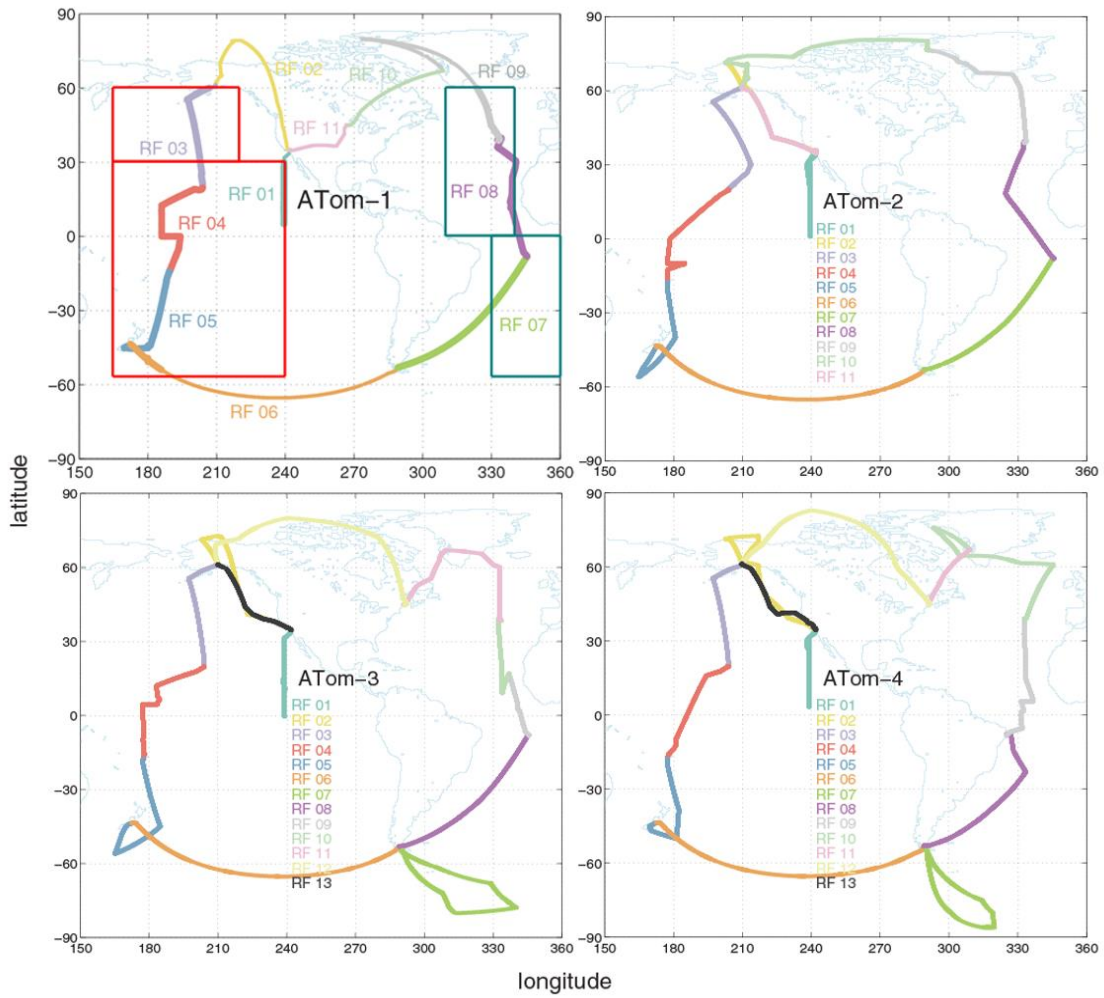


**Figure S1.** Flight tracks for the 4 ATom deployments. For ATom-1, the flight segments considered Pacific and Atlantic domains for this paper are shown with very thick lines. The corresponding blocks used for model climatologies are outlined with rectangles: Pacific, red; Atlantic, blue-green.

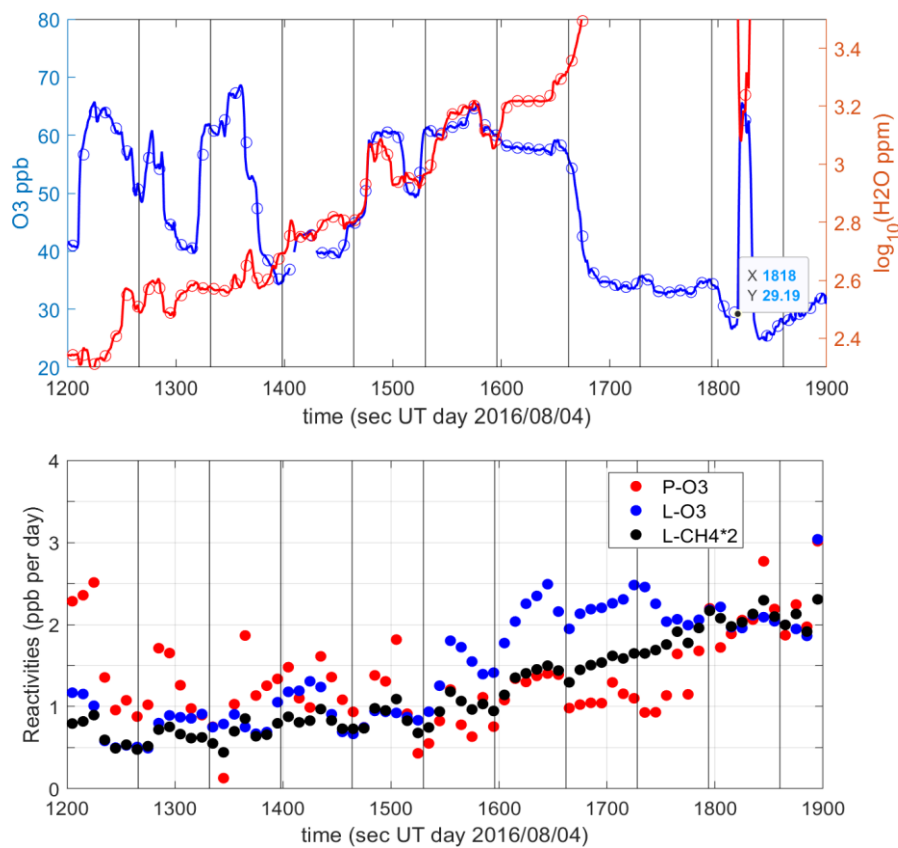


**Figure S2.** Profile during a descent on the Anchorage-Kona flight (ATom-1, RF-3, 31°N). The profile here begins at 7.2 km (1200 s) and ends at 2.1 km (1900 s, H<sub>2</sub>O is cut off). (a) Fine structure in O<sub>3</sub> (ppb) and H<sub>2</sub>O (log<sub>10</sub>, ppm) at 1-sec (solid line) and 10 s (open circles) resolution. (b) Reactivities for the 10 s parcels calculated with the UCI CTM. Descent rate averaged 7.5 m/s, and vertical lines indicate 500 m thick layers.

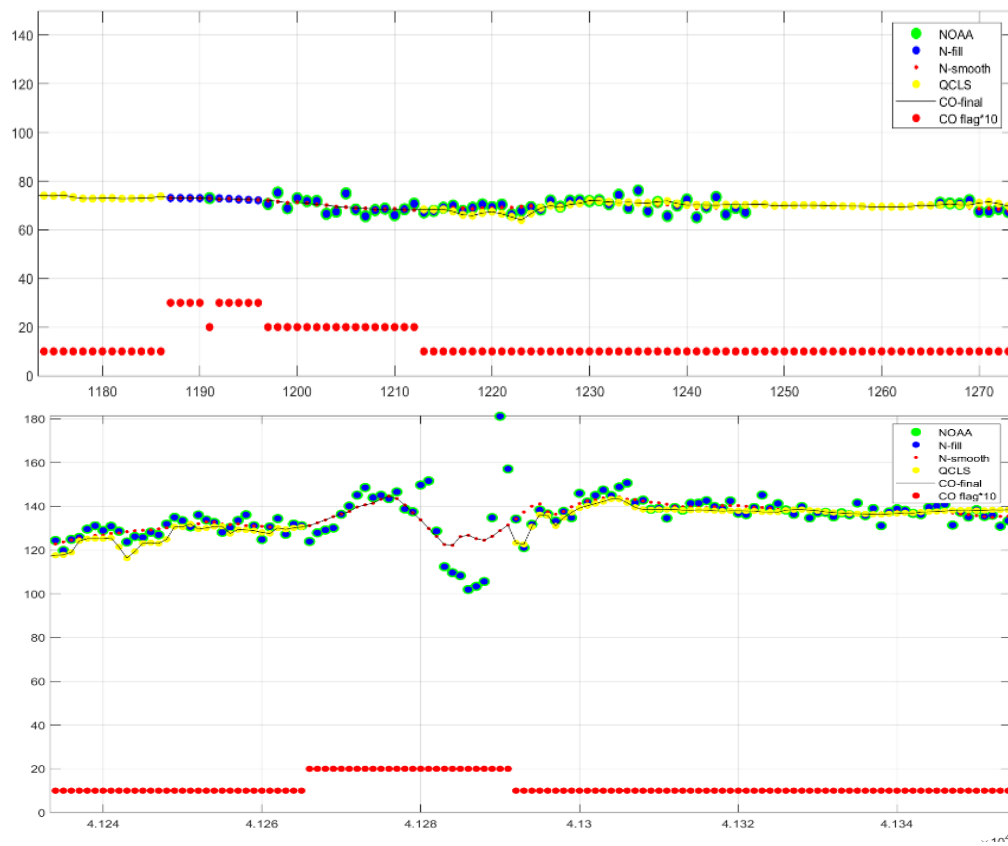


**Figure S3.** Example of CO time series showing all the intermediate CO products and flags. See legend and text.

408

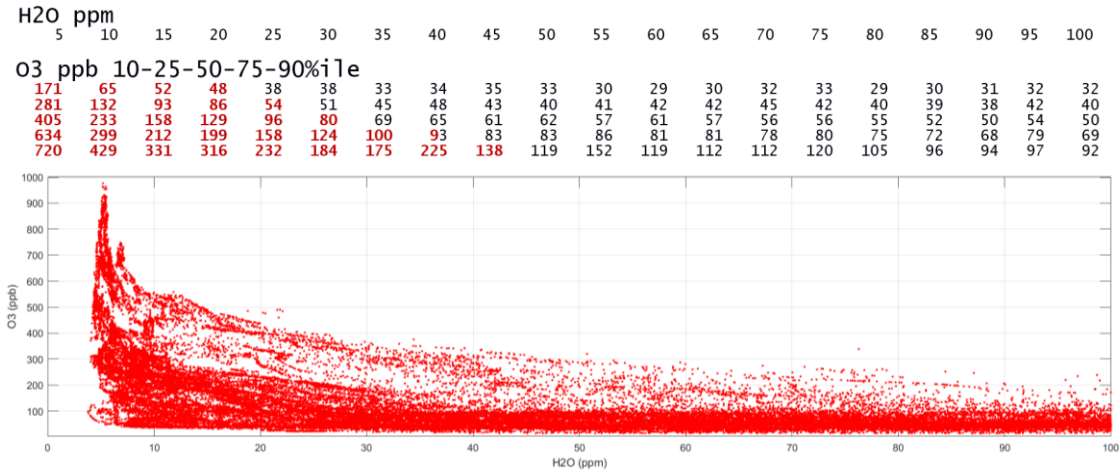


**Figure S4a.** Scatter plot of O<sub>3</sub> (ppb) and H<sub>2</sub>O (ppm) for all ATom deployments, filtered by H<sub>2</sub>O < 100 ppm. The percentiles (10-25-50-75-90 %ile) of O<sub>3</sub> in each 5-ppm-wide bin starting at 5 ppm (= 2.5–7.5 ppm) ending at 100 pm in in the table at the top of this figure. Stratospheric influence (red) is clearly seen in the median for <30 ppm.

409

410

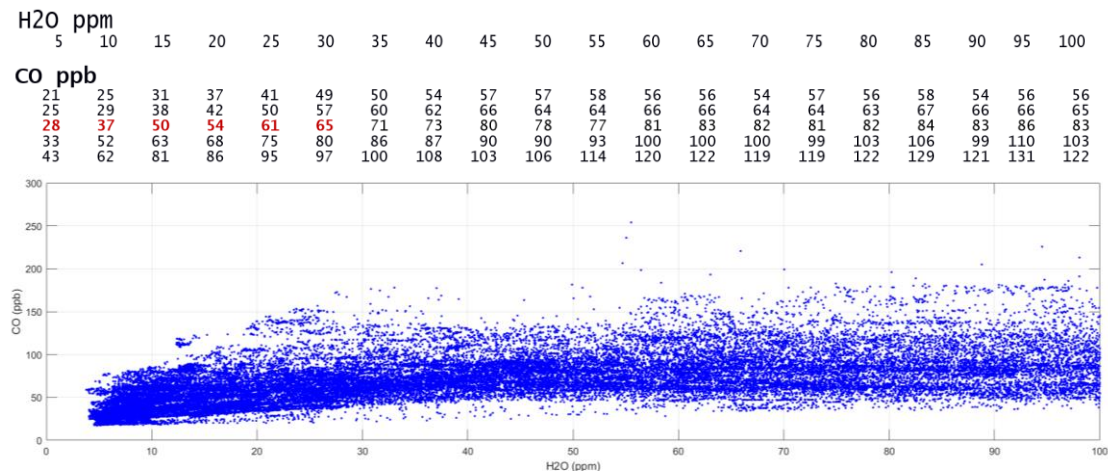


**Figure S4b.** Scatter plot of CO (ppb) and H<sub>2</sub>O (ppm) for all ATom deployments, filtered by H<sub>2</sub>O < 100 ppm. See Figure S4a.

411



412

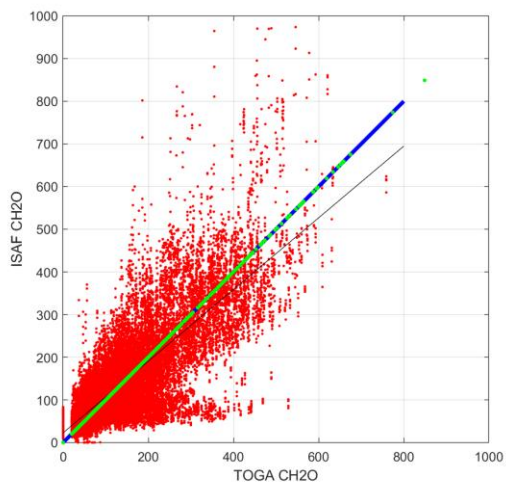


**Figure S5.** Scatter plot of coincident HCHO measurements (ppb) from ISAF and TOGA for all ATom deployments. The thick blue-green line is the 1:1 relationship and the thin black line shows a linear regression of ISAF vs. TOGA. Notably, ISAF has more frequent high values >600 ppb, with some above 1000 ppb (not shown).

413

ATom research flights in the Mor.2020-05-27...tbl (149,133 parcels)							Airport removed (146,494 parcels)	
ATom deployment	Research Flight no.	ATom flight	Airports	parcel begin	parcel end	YYYYMMDD	parcel begin	parcel end
1	1	1	PMD PMD*	1	3380	20160729	1	3333
1	2	2	PMD ANC	3381	7038	20160801	3334	6939
1	3	3	ANC KOA	7039	9658	20160803	6940	9526
1	4	4	KOA PPG	9659	12760	20160806	9527	12583
1	5	5	PPG CHC	12761	15141	20160808	12584	14917
1	6	6	CHC PUQ	15142	18976	20160812	14918	18692
1	7	7	PUQ ASI	18977	22355	20160815	18693	21998
1	8	8	ASI TER	22356	25431	20160817	21999	25040
1	9	9	TER SFJ	25432	28976	20160820	25041	28544
1	10	10	SFJ MSP	28977	31127	20160822	28545	30663
1	11	11	MSP PMD	31128	32899	20160823	30664	32383
2	1	12	PMD PMD*	32900	36621	20170126	32384	36061
2	2	13	PMD ANC	36622	40115	20170129	36062	39480
2	3	14	ANC KOA	40116	43062	20170201	39481	42360
2	4	15	KOA NAN	43063	46470	20170203	42361	45717
2	5	16	NAN CHC	46471	49562	20170205	45718	48774
2	6	17	CHC PUQ	49563	53116	20170210	48775	52267
2	7	18	PUQ ASI	53117	56358	20170213	52268	55390
2	8	19	ASI TER	56359	59468	20170215	55391	58446
2	9	20	TER THU	59469	62151	20170218	58447	61088
2	10	21	THU ANC	62152	64893	20170219	61089	63762
2	11	22	ANC PMD	64894	66978	20170221	63763	65807
3	1	23	PMD PMD*	66979	70683	20170928	65808	69465
3	2	24	PMD ANC	70684	74281	20171001	69466	73001
3	3	25	ANC KOA	74282	76949	20171004	73002	75608
3	4	26	KOA NAN	76950	80163	20171006	75609	78754
3	5	27	NAN CHC	80164	83472	20171008	78755	82000
3	6	28	CHC PUQ	83473	87028	20171011	82001	85462
3	7	29	PUQ PUQ^	87029	90872	20171014	85463	89225
3	8	30	PUQ ASI	90873	94279	20171017	89226	92576
3	9	31	ASI SID	94280	95928	20171019	92577	94191
3	10	32	SID TER	95929	98695	20171020	94192	96916
3	11	33	TER BGR	98696	102094	20171023	96917	100272
3	12	34	BGR ANC	102095	105540	20171025	100273	103677
3	13	35	ANC PMD	105541	107873	20171027	103678	105983
4	1	36	PMD PMD*	107874	111294	20180424	105984	109357
4	2	37	PMD ANC	111295	115012	20180427	109358	113028
4	3	38	ANC KOA	115013	117934	20180429	113029	115847
4	4	39	KOA NAN	117935	120880	20180501	115848	118741
4	5	40	NAN CHC	120881	123717	20180503	118742	121542
4	6	41	CHC PUQ	123718	127370	20180506	121543	125122
4	7	42	PUQ PUQ^	127371	131238	20180509	125123	128934
4	8	43	PUQ REC	131239	134829	20180512	128935	132463
4	9	44	REC TER	134830	138214	20180514	132464	135770
4	10	45	TER SFJ	138215	141697	20180517	135771	139210
4	11	46	SFJ BGR	141698	142846	20180518	139211	140316
4	12	47	BGR ANC	142847	146670	20180519	140317	144095
4	13	48	ANC PMD	146671	149133	20180521	144096	146494

\* 4 flights to equator following 120W. ^ 2 flights to 80S and 86S over Antarctica.

<b>Table S2. MDS data and source</b>			
<b>id#</b>	<b>MDS data designation</b>	<b>Description</b>	<b>ATom source name</b>
1	parcel_M	Unique sequential parcel number for all MDS 10s data, beginning 1,000,001	
2	ATno	ATom deployment number (1:4)	A.no
3	RFno	Research Flight number (1:11, 1:11, 1:13, 1:13)	RF
4	RRno	RF number across all of ATom (1:48)	
5	YYMMDD	Date (UT) of the start of each RF	YYMMDD
6	UTC_M	Start time in sec relative to Date for each 10s parcel	UTC_Start
7	Lat_M	Latitude (-90:+90)	G_LAT
8	Lng_M	Longitude (-180:+180)	G_LONG
9	Alt_M	Altitude (m above mean sea level)	G_ALT
10	P_M	Pressure (hPa)	P
11	T_M	Temperture (K)	T
12	H2O_M	water, ppm (all dry air mole fraction)	H2O_DLH
13	RHw_M	relative humidity over liquid water (%)	RHw_DLH
14	O3_M	ozone, ppb	O3_CL
15	CO_M	carbon monoxide, ppb	(1) CO_QCLS, (2) CO_NOAA
16	CH4_M	methane, ppb	(1) CH4_NOAA, (2) CH4_QCLS
17	NOx_M	odd-nitrogen, NO+NO2, ppt	NO_CL + NO2_CL
18	NOxPSS_M	odd-nitrogen, with photo-stationary state NO2, ppt	NOx_PSS
19	HNO3_M	nitric acid, HONO2, ppt	HNO3_CIT
20	HNO4_M	pernitric acid, HO2NO2, ppt	PNA_CIT
21	PAN_M	peroxyacetyl nitrate, C2H3NO5 - CH3C(O)OONO2, ppt	(1) PAN_GTCIMS, (2) PAN_PECDD*
22	CH2O_M	formaldehyde, HCHO, ppt	(1) CH2O_ISAF, (2) CH2O_TOGA
23	H2O2_M	hydrogen peroxide, HOOH, ppt	H2O2_CIT
24	CH3OOH_M	methyl hydrogen peroxide, ppt	MHP_CIT
25	Acetone_M	acetone, CH3C(O)CH3, ppt	Acetone_TOGA
26	Acetald_M	acetaldehyde, CH3C(O)H, ppt	CH3CHO_TOGA
27	C2H6_M	ethane, C2H6, ppt	Ethane_WAS
28	C3H8_M	propane, C3H8, ppt	(1) Propane_WAS, (2) Propane_TOGA
29	iC4H10_M	iso-butane, iC4H10, ppt	(1) iButane_WAS, (2) iButane_TOGA
30	nC4H10_M	n-butane, nC4H10, ppt	(1) nButane_WAS, (2) nButane_TOGA
31	Alkanes_M	pentane (C5H12) and higher, ppt	iPentane_WAS + nPentane_WAS + nHexane_WAS + nHeptane_WAS + x2MePentane_WAS + x3MePentane_WAS
32	C2H4_M	ethene, C2H4, ppt	Ethene_WAS
33	Alkenes_M	propene (C3H6) and higher, ppt	Propene_WAS
34	C2H2_M	acetylene (ethyne), C2H2, ppt	Ethyne_WAS
35	C5H8_M	isoprene, C5H8, ppt	(1) Isoprene_TOGA, (2) Isoprene_WAS
36	Benzene_M	benzene, C6H6, ppt	(1) Benzene_TOGA, (2) Benzene_WAS*

37	Toluene_M	methylbenzene, C7H8, ppt	(1) Toluene_TOGA+EthBenzene_TOGA, (2) Toluene_WAS + EthBenzene_WAS
38	Xylene_M	dimethylbenzene, C8H10, ppt	(1) mpXylene_TOGA+oXylene_TOGA, (2) mpXylene_WAS+oXylene_WAS
39	MeONO2_M	methyl nitrate, CH3ONO2, ppt	MeONO2_WAS
40	EtONO2_M	ethyl nitrate, CH3ONO2, ppt	EthONO2_WAS
41	RONO2_M	higher organo nitrates, R=C3+, ppt	iPropONO2_WAS + nPropONO2_WAS + x2ButONO2_WAS + x3PentONO2_WAS + x2PentONO2_WAS + x3Me2ButONO2_WAS
42	MeOH_M	methanol, CH3OH, ppt	CH3OH_TOGA
43	HCN_M	hydrogen cyanide, ppt	(1) HCN_CIT, (2) HCN_TOGA
44	CH3CN_M	acetonitrile (methyl cyanide), CH3CN, ppt	CH3CN_TOGA
45	SF6_M	sulfure hexafluoride, ppt	(1) SF6_PECD, (2) SF6_UCATS
46	S_nuc_M	particle surface area (um <sup>2</sup> /cm <sup>3</sup> ), nucleation: 0.0027 < Dp <= 0.012 um	S_nucl_AMP
47	S_atk_M	particle surface area (um <sup>2</sup> /cm <sup>3</sup> ), Aitken: 0.012 < Dp <=0.06 um	S_aitken_AMP
48	S_acc_M	particle surface area (um <sup>2</sup> /cm <sup>3</sup> ), accumulation: 0.06 < Dp <=0.50 um	S_accum_AMP
49	S_crs_M	particle surface area (um <sup>2</sup> /cm <sup>3</sup> ), coarse: 0.50 < Dp <=4.8 um	S_coarse_AMP
50	CloudInd_M	cloud indicator (0:4), dimensionless	cloudindicator_CAPS
<p>Note: The flag value, flag_M(:,1:50) is indexed to the 50 variables above. Only flag_M(:,10:50) have meaningful values. The flag values are: 0 (NaNs, only in research flight 46), 1 (primary data), 2 (secondary data), 3 (short-gap interpolation), 4 (long-gap interpolation for troposphere), 5 (missing flight filled) and 6 (long-gap interpolation for stratosphere) are described in text.</p>			

417

<b>RRno</b>	<b>1</b>	<b>2</b>	<b>3</b>	<b>4</b>	<b>5</b>	<b>6</b>	<b>7</b>	<b>8</b>	<b>9</b>	<b>10</b>	<b>11</b>
<Lat> (deg)	20	62	42	4	-34	-58	-32	18	65	55	38
<Lng> (deg)	-120	-133	-158	-169	-83	-87	-37	-21	-49	-78	-104
<Alt> (m)	7055	8092	7118	6143	6634	7034	6761	6494	6930	6090	7736
<b># parcels</b>	<b>3333</b>	<b>3606</b>	<b>2587</b>	<b>3057</b>	<b>2334</b>	<b>3775</b>	<b>3306</b>	<b>3042</b>	<b>3504</b>	<b>2119</b>	<b>1720</b>
H2O_M	100%	100%	100%	100%	100%	100%	100%	100%	100%	100%	100%
RHw_M	100%	100%	100%	100%	100%	100%	100%	100%	100%	100%	100%
O3_M	99%	99%	100%	99%	100%	100%	99%	100%	100%	100%	100%
CO_M	100%	100%	100%	100%	100%	100%	100%	100%	100%	100%	100%
CH4_M	54%	95%	95%	94%	86%	93%	94%	92%	95%	95%	93%
NOx_M	90%	94%	91%	84%	91%	85%	96%	98%	89%	95%	94%
NOxPSS_M	94%	91%	91%	86%	88%	28%	67%	95%	88%	95%	92%
HNO3_M	92%	96%	97%	92%	0%	95%	95%	97%	96%	97%	97%
HNO4_M	59%	87%	74%	67%	0%	90%	85%	67%	88%	73%	66%
PAN_M	78%	67%	48%	90%	40%	87%	97%	93%	98%	92%	95%
CH2O_M	99%	100%	100%	100%	100%	100%	100%	100%	100%	100%	100%
H2O2_M	92%	96%	97%	92%	0%	95%	95%	97%	96%	97%	97%
CH3OOH_M	56%	69%	81%	83%	84%	79%	81%	82%	82%	79%	79%
Acetone_M	89%	92%	88%	98%	92%	90%	93%	94%	94%	94%	94%
Acetald_M	89%	92%	88%	98%	90%	90%	90%	94%	93%	94%	94%
C2H6_M	50%	32%	43%	44%	62%	37%	39%	43%	40%	46%	45%
C3H8_M	90%	95%	92%	97%	97%	95%	96%	97%	96%	98%	95%
iC4H10_M	95%	95%	92%	98%	97%	95%	96%	97%	98%	98%	96%
nC4H10_M	95%	95%	92%	98%	97%	95%	96%	97%	98%	98%	96%
Alkanes_M	50%	32%	43%	44%	62%	37%	39%	43%	40%	46%	45%
C2H4_M	50%	32%	43%	44%	62%	37%	39%	43%	40%	46%	45%
Alkenes_M	50%	32%	43%	44%	62%	37%	39%	43%	40%	46%	45%
C2H2_M	50%	32%	43%	44%	62%	37%	39%	43%	40%	46%	45%
C5H8_M	95%	95%	92%	98%	97%	95%	96%	97%	98%	98%	96%
Benzene_M	95%	95%	92%	98%	97%	95%	96%	97%	98%	98%	96%
Toluene_M	100%	99%	94%	98%	98%	99%	100%	99%	100%	100%	99%
Xylene_M	100%	99%	94%	98%	98%	99%	100%	99%	100%	100%	99%
MeONO2_M	50%	32%	43%	44%	55%	37%	39%	43%	33%	43%	43%
EtONO2_M	50%	31%	40%	43%	47%	28%	34%	42%	31%	39%	39%
RONO2_M	50%	32%	43%	44%	62%	37%	39%	43%	40%	46%	45%
MeOH_M	89%	92%	88%	98%	92%	90%	92%	92%	92%	94%	94%
HCN_M	98%	100%	100%	100%	92%	100%	100%	100%	100%	100%	100%
CH3CN_M	89%	92%	88%	98%	92%	90%	93%	94%	94%	94%	91%
SF6_M	90%	88%	98%	92%	91%	80%	96%	79%	99%	90%	84%
S_nuc_M	95%	92%	93%	99%	92%	87%	91%	94%	91%	88%	93%
S_atk_M	95%	92%	93%	99%	92%	87%	91%	94%	91%	88%	93%
S_acc_M	95%	92%	93%	99%	92%	87%	91%	93%	91%	88%	93%
S_crs_M	95%	92%	93%	99%	92%	87%	91%	93%	91%	88%	93%
CloudInd_M	100%	100%	100%	100%	99%	100%	100%	100%	100%	100%	100%

<b>RRno</b>	<b>12</b>	<b>13</b>	<b>14</b>	<b>15</b>	<b>16</b>	<b>17</b>	<b>18</b>	<b>19</b>	<b>20</b>	<b>21</b>	<b>22</b>
<Lat> (deg)	18	55	40	0	-41	-58	-32	15	60	73	45
<Lng> (deg)	-120	-142	-154	-46	138	-89	-37	-28	-38	-129	-135
<Alt> (m)	8477	6915	5726	7514	7233	7629	8835	6832	5869	5553	6969
<b># parcels</b>	<b>3678</b>	<b>3419</b>	<b>2880</b>	<b>3357</b>	<b>3057</b>	<b>3493</b>	<b>3123</b>	<b>3056</b>	<b>2642</b>	<b>2674</b>	<b>2045</b>
H2O_M	100%	100%	100%	100%	100%	100%	100%	100%	100%	100%	100%
RHw_M	100%	100%	100%	100%	100%	100%	100%	100%	100%	100%	100%
O3_M	99%	100%	100%	100%	100%	100%	100%	100%	100%	100%	100%
CO_M	100%	100%	100%	100%	100%	100%	100%	100%	100%	100%	100%
CH4_M	100%	100%	100%	99%	98%	99%	100%	100%	100%	99%	100%
NOx_M	85%	89%	100%	95%	82%	82%	87%	80%	82%	100%	96%
NOxPSS_M											
HNO3_M	90%	0%	91%	95%	96%	92%	97%	97%	97%	93%	98%
HNO4_M	82%	0%	77%	70%	77%	81%	87%	77%	87%	93%	94%
PAN_M	84%	100%	100%	95%	100%	100%	99%	97%	94%	100%	94%
CH2O_M	100%	100%	100%	100%	100%	100%	100%	100%	100%	100%	100%
H2O2_M	90%	0%	91%	95%	96%	92%	97%	97%	97%	93%	98%
CH3OOH_M	67%	62%	71%	67%	65%	58%	58%	59%	58%	60%	56%
Acetone_M	91%	92%	85%	97%	96%	93%	95%	96%	89%	91%	94%
Acetald_M	91%	92%	85%	97%	96%	93%	95%	97%	89%	91%	94%
C2H6_M	38%	28%	45%	36%	42%	43%	40%	47%	56%	58%	61%
C3H8_M	95%	88%	81%	94%	94%	93%	87%	87%	87%	58%	88%
iC4H10_M	97%	94%	91%	97%	97%	95%	95%	97%	94%	95%	97%
nC4H10_M	97%	94%	91%	97%	97%	95%	95%	97%	94%	95%	97%
Alkanes_M	38%	28%	45%	36%	42%	43%	40%	47%	56%	58%	61%
C2H4_M	38%	28%	45%	36%	42%	43%	40%	47%	56%	58%	61%
Alkenes_M	38%	28%	45%	36%	42%	43%	40%	47%	56%	58%	61%
C2H2_M	38%	28%	45%	36%	42%	43%	40%	47%	56%	58%	61%
C5H8_M	97%	94%	93%	97%	97%	95%	96%	98%	94%	96%	97%
Benzene_M	97%	94%	93%	97%	97%	95%	96%	98%	94%	96%	97%
Toluene_M	100%	96%	96%	100%	100%	100%	100%	100%	98%	100%	100%
Xylene_M	100%	96%	96%	100%	100%	100%	100%	100%	98%	100%	100%
MeONO2_M	37%	26%	45%	36%	38%	35%	40%	47%	53%	54%	51%
EtONO2_M	37%	26%	45%	36%	38%	35%	40%	47%	52%	54%	50%
RONO2_M	38%	28%	45%	36%	42%	43%	40%	47%	56%	58%	61%
MeOH_M	90%	92%	83%	97%	92%	93%	95%	97%	89%	91%	94%
HCN_M	99%	89%	100%	100%	100%	98%	100%	100%	100%	93%	100%
CH3CN_M	91%	92%	85%	97%	96%	93%	95%	97%	89%	87%	94%
SF6_M	87%	97%	96%	88%	98%	99%	98%	99%	99%	99%	69%
S_nuc_M	86%	81%	98%	95%	85%	95%	85%	98%	75%	89%	91%
S_atk_M	86%	81%	98%	95%	85%	95%	85%	98%	75%	89%	91%
S_acc_M	86%	81%	97%	95%	84%	95%	85%	98%	75%	88%	91%
S_crs_M	86%	81%	97%	95%	84%	95%	85%	98%	75%	88%	91%
CloudInd_M	100%	100%	100%	97%	100%	100%	100%	100%	100%	100%	100%

<b>RRno</b>	<b>23</b>	<b>24</b>	<b>25</b>	<b>26</b>	<b>27</b>	<b>28</b>	<b>29</b>	<b>30</b>	<b>31</b>	<b>32</b>	<b>33</b>	<b>34</b>	<b>35</b>
<Lat> (deg)	18	55	42	4	-41	-58	-67	-32	4	22	55	67	46
<Lng> (deg)	-121	-141	-158	-14	63	-91	-50	-36	-19	-26	-43	-105	-136
<Alt> (m)	8988	7623	6720	6781	6844	6836	7263	8169	6678	6329	5522	6231	6033
<b># parcels</b>	<b>3658</b>	<b>3536</b>	<b>2607</b>	<b>3146</b>	<b>3246</b>	<b>3462</b>	<b>3763</b>	<b>3351</b>	<b>1615</b>	<b>2725</b>	<b>3356</b>	<b>3405</b>	<b>2306</b>
H2O_M	100%	100%	100%	100%	100%	100%	100%	100%	100%	100%	100%	100%	100%
RHw_M	100%	100%	100%	100%	100%	100%	100%	100%	100%	100%	100%	100%	100%
O3_M	99%	100%	100%	100%	100%	100%	100%	100%	89%	99%	100%	100%	100%
CO_M	100%	100%	100%	100%	100%	100%	100%	100%	100%	100%	100%	100%	100%
CH4_M	100%	98%	100%	100%	100%	100%	100%	100%	100%	100%	100%	100%	100%
NOx_M	0%	98%	100%	100%	97%	100%	87%	94%	89%	94%	99%	100%	100%
NOxPSS_M													
HNO3_M	96%	96%	96%	95%	97%	91%	94%	96%	91%	85%	97%	90%	66%
HNO4_M	0%	0%	0%	0%	0%	0%	0%	0%	0%	0%	0%	0%	0%
PAN_M	100%	100%	100%	98%	100%	100%	99%	99%	100%	98%	100%	98%	100%
CH2O_M	100%	100%	100%	100%	100%	100%	98%	100%	100%	100%	100%	100%	100%
H2O2_M	96%	96%	96%	95%	97%	91%	94%	96%	91%	85%	97%	90%	95%
CH3OOH_M	61%	59%	59%	60%	58%	58%	59%	61%	58%	53%	67%	60%	64%
Acetone_M	94%	95%	87%	95%	96%	97%	92%	96%	86%	93%	94%	98%	98%
Acetald_M	94%	95%	87%	97%	97%	97%	92%	96%	86%	96%	94%	98%	98%
C2H6_M	46%	47%	61%	57%	52%	48%	33%	33%	36%	33%	40%	39%	50%
C3H8_M	95%	97%	94%	98%	98%	98%	95%	97%	92%	96%	94%	98%	98%
iC4H10_M	95%	97%	94%	99%	98%	98%	95%	97%	91%	96%	94%	98%	98%
nC4H10_M	95%	97%	94%	99%	98%	98%	95%	97%	91%	96%	94%	98%	98%
Alkanes_M	46%	47%	61%	57%	52%	48%	34%	34%	39%	33%	40%	39%	50%
C2H4_M	46%	47%	61%	57%	52%	48%	34%	34%	39%	33%	40%	39%	50%
Alkenes_M	46%	47%	61%	57%	52%	48%	34%	34%	39%	33%	40%	39%	50%
C2H2_M	46%	47%	61%	57%	46%	46%	34%	33%	39%	33%	40%	39%	50%
C5H8_M	95%	97%	94%	99%	98%	98%	95%	97%	92%	96%	94%	98%	98%
Benzene_M	95%	97%	94%	99%	98%	98%	95%	97%	92%	96%	94%	98%	98%
Toluene_M	100%	100%	95%	100%	100%	100%	99%	100%	95%	100%	100%	100%	100%
Xylene_M	100%	100%	95%	100%	100%	100%	99%	100%	95%	100%	100%	100%	100%
MeONO2_M	46%	47%	61%	57%	52%	48%	34%	34%	39%	33%	40%	39%	50%
EtONO2_M	46%	47%	61%	57%	52%	48%	34%	34%	39%	33%	40%	39%	50%
RONO2_M	46%	47%	61%	57%	52%	48%	34%	34%	39%	33%	40%	39%	50%
MeOH_M	94%	95%	87%	97%	97%	97%	92%	96%	86%	96%	94%	98%	98%
HCN_M	100%	99%	100%	100%	100%	100%	100%	100%	100%	100%	100%	100%	100%
CH3CN_M	94%	95%	87%	96%	95%	97%	92%	96%	86%	95%	94%	98%	98%
SF6_M	77%	100%	76%	84%	60%	96%	95%	83%	91%	99%	97%	82%	92%
S_nuc_M	92%	77%	74%	94%	91%	86%	92%	91%	99%	88%	91%	81%	92%
S_atk_M	92%	77%	74%	94%	91%	86%	92%	91%	99%	88%	91%	81%	92%
S_acc_M	92%	77%	67%	94%	91%	86%	91%	91%	99%	88%	91%	81%	91%
S_crs_M	92%	77%	67%	94%	91%	86%	91%	91%	99%	88%	91%	81%	91%
CloudInd_M	98%	100%	100%	100%	100%	100%	100%	100%	100%	100%	100%	99%	100%

<b>RRno</b>	<b>36</b>	<b>37</b>	<b>38</b>	<b>39</b>	<b>40</b>	<b>41</b>	<b>42</b>	<b>43</b>	<b>44</b>	<b>45</b>	<b>46</b>	<b>47</b>	<b>48</b>
<Lat> (deg)	19	56	42	3	-38	-59	-70	-32	13	60	56	67	46
<Lng> (deg)	-121	-141	-158	-132	10	-93	-59	-41	-27	-37	-62	-105	-135
<Alt> (m)	8278	6678	6123	6419	5922	6843	7197	6672	6729	7019	9678	6759	5935
<b># parcels</b>	<b>3374</b>	<b>3671</b>	<b>2819</b>	<b>2894</b>	<b>2801</b>	<b>3580</b>	<b>3812</b>	<b>3529</b>	<b>3307</b>	<b>3440</b>	<b>1106</b>	<b>3779</b>	<b>2399</b>
H2O_M	100%	100%	100%	100%	100%	100%	100%	100%	100%	100%	100%	100%	100%
RHw_M	100%	100%	100%	100%	100%	100%	100%	100%	100%	100%	100%	100%	100%
O3_M	100%	100%	100%	100%	100%	100%	99%	100%	100%	100%	0%	100%	100%
CO_M	100%	100%	100%	100%	100%	100%	100%	100%	100%	100%	100%	100%	100%
CH4_M	100%	100%	100%	100%	100%	100%	100%	100%	100%	100%	100%	100%	100%
NOx_M	62%	77%	93%	84%	99%	100%	89%	100%	100%	99%	100%	100%	100%
NOxPSS_M													
HNO3_M	93%	94%	98%	75%	95%	96%	96%	96%	96%	97%	96%	96%	98%
HNO4_M	0%	0%	0%	0%	0%	0%	0%	0%	0%	0%	0%	0%	0%
PAN_M	99%	92%	100%	100%	99%	100%	100%	100%	100%	100%	83%	100%	100%
CH2O_M	100%	82%	100%	100%	98%	100%	98%	98%	98%	96%	0%	95%	93%
H2O2_M	94%	94%	98%	75%	95%	96%	96%	96%	96%	97%	96%	96%	98%
CH3OOH_M	43%	59%	59%	59%	0%	0%	0%	0%	0%	69%	67%	0%	0%
Acetone_M	96%	98%	98%	88%	98%	96%	98%	98%	98%	97%	0%	95%	93%
Acetald_M	96%	87%	97%	88%	92%	91%	94%	97%	93%	89%	0%	95%	92%
C2H6_M	26%	35%	40%	40%	46%	34%	31%	28%	31%	29%	0%	27%	31%
C3H8_M	96%	99%	99%	94%	100%	97%	98%	98%	98%	97%	0%	96%	95%
iC4H10_M	96%	99%	99%	94%	100%	97%	98%	98%	98%	97%	0%	96%	95%
nC4H10_M	96%	99%	99%	94%	100%	97%	98%	98%	98%	97%	0%	96%	95%
Alkanes_M	26%	35%	42%	43%	46%	34%	33%	28%	31%	29%	0%	27%	31%
C2H4_M	26%	35%	42%	43%	46%	34%	33%	28%	31%	29%	0%	27%	31%
Alkenes_M	26%	35%	42%	43%	46%	34%	33%	28%	31%	29%	0%	27%	31%
C2H2_M	26%	35%	42%	43%	46%	34%	33%	28%	31%	29%	0%	27%	31%
C5H8_M	96%	99%	99%	94%	100%	97%	98%	98%	98%	97%	0%	96%	95%
Benzene_M	96%	99%	99%	94%	100%	97%	98%	98%	98%	97%	0%	96%	95%
Toluene_M	100%	100%	99%	95%	100%	100%	100%	100%	100%	100%	0%	100%	100%
Xylene_M	100%	100%	99%	95%	100%	100%	100%	100%	100%	100%	0%	100%	100%
MeONO2_M	26%	35%	42%	43%	46%	34%	33%	28%	31%	29%	0%	27%	31%
EtONO2_M	26%	35%	42%	43%	46%	34%	33%	28%	31%	29%	0%	27%	31%
RONO2_M	26%	35%	42%	43%	46%	34%	33%	28%	31%	29%	0%	27%	31%
MeOH_M	96%	98%	98%	88%	98%	96%	98%	98%	98%	97%	0%	95%	93%
HCN_M	99%	100%	100%	95%	99%	100%	100%	99%	99%	100%	96%	100%	100%
CH3CN_M	96%	98%	98%	88%	98%	96%	98%	98%	98%	97%	0%	95%	93%
SF6_M	76%	92%	97%	95%	97%	85%	90%	98%	88%	85%	94%	97%	94%
S_nuc_M	94%	99%	89%	94%	96%	82%	81%	96%	98%	65%	85%	93%	94%
S_atk_M	94%	99%	89%	94%	96%	82%	81%	96%	98%	65%	85%	93%	94%
S_acc_M	94%	99%	88%	94%	96%	82%	81%	95%	98%	65%	85%	92%	94%
S_crs_M	94%	99%	88%	94%	96%	82%	81%	95%	98%	65%	85%	92%	94%
CloudInd_M	100%	100%	100%	100%	100%	100%	99%	94%	100%	100%	100%	100%	99%



<b>Table S4.</b> ATom, % of records by flag							
<b>Flags</b>	<b>0*</b>	<b>1</b>	<b>2</b>	<b>3</b>	<b>4</b>	<b>5</b>	<b>6</b>
H2O_M	0.8%	99.0%	0.0%	0.3%	0.0%	0.0%	0.0%
RHw_M	0.8%	99.0%	0.0%	0.3%	0.0%	0.0%	0.0%
O3_M	0.8%	98.6%	0.0%	0.3%	0.3%	0.0%	0.0%
CO_M	0.8%	79.4%	19.4%	0.1%	0.5%	0.0%	0.0%
CH4_M	0.8%	93.5%	1.3%	1.9%	2.5%	0.0%	0.0%
NOx_M	0.8%	80.8%	0.0%	8.3%	7.6%	2.5%	0.0%
NOxPSS_M	0.8%	82.4%	0.0%	11.8%	5.1%	0.0%	0.0%
HNO3_M	0.8%	78.0%	0.0%	11.6%	5.7%	3.9%	0.0%
HNO4_M	0.8%	28.5%	0.0%	4.0%	8.5%	58.3%	0.0%
PAN_M	0.8%	58.0%	28.4%	7.5%	5.4%	0.0%	0.0%
CH2O_M	0.8%	82.9%	14.9%	0.3%	1.1%	0.0%	0.0%
H2O2_M	0.8%	78.5%	0.0%	11.6%	5.3%	3.9%	0.0%
CH3OOH_M	0.8%	42.0%	0.0%	12.0%	29.4%	15.8%	0.0%
Acetone_M	0.8%	31.7%	0.0%	61.6%	6.0%	0.0%	0.0%
Acetald_M	0.8%	31.4%	0.0%	60.9%	6.9%	0.0%	0.0%
C2H6_M	0.8%	28.0%	0.0%	12.4%	56.3%	0.0%	2.5%
C3H8_M	0.8%	28.0%	53.1%	12.5%	5.1%	0.0%	0.7%
iC4H10_M	0.8%	28.1%	54.9%	12.5%	3.2%	0.0%	0.5%
nC4H10_M	0.8%	28.1%	54.9%	12.5%	3.2%	0.0%	0.5%
Alkanes_M	0.8%	28.1%	0.0%	12.5%	56.0%	0.0%	2.6%
C2H4_M	0.8%	28.1%	0.0%	12.5%	56.0%	0.0%	2.6%
Alkenes_M	0.8%	28.1%	0.0%	12.5%	56.0%	0.0%	2.6%
C2H2_M	0.8%	28.0%	0.0%	12.5%	56.2%	0.0%	2.6%
C5H8_M	0.8%	31.8%	2.3%	61.7%	3.1%	0.0%	0.5%
Benzene_M	0.8%	31.8%	2.3%	61.7%	3.1%	0.0%	0.5%
Toluene_M	0.8%	33.0%	0.6%	64.8%	0.6%	0.0%	0.2%
Xylene_M	0.8%	33.0%	0.6%	64.8%	0.6%	0.0%	0.2%
MeONO2_M	0.8%	27.4%	0.0%	12.3%	57.0%	0.0%	2.6%
EtONO2_M	0.8%	26.8%	0.0%	12.1%	57.8%	0.0%	2.6%
RONO2_M	0.8%	28.1%	0.0%	12.5%	56.0%	0.0%	2.6%
MeOH_M	0.8%	31.7%	0.0%	61.5%	6.0%	0.0%	0.0%
HCN_M	0.8%	78.5%	8.3%	11.6%	0.8%	0.0%	0.0%
CH3CN_M	0.8%	31.7%	0.0%	61.5%	6.0%	0.0%	0.0%
SF6_M	0.8%	10.4%	5.8%	79.2%	3.8%	0.0%	0.0%
S_nuc_M	0.8%	84.6%	0.0%	4.4%	10.3%	0.0%	0.0%
S_atk_M	0.8%	84.6%	0.0%	4.4%	10.3%	0.0%	0.0%
S_acc_M	0.8%	84.1%	0.0%	4.6%	10.6%	0.0%	0.0%
S_crs_M	0.8%	84.1%	0.0%	4.6%	10.6%	0.0%	0.0%
CloudInd_M	0.8%	98.7%	0.0%	0.2%	0.3%	0.0%	0.0%

\* The 0.8% flag=0 corresponds to the short flight RF #46, for which we NaN'd all chemical data.

<b>Table S5. Test of long-gap interpolation method</b>				
Species	All parcels	Long-gap interpolated parcels		Short-gap fill
(ppt unless noted)	mean	bias (% of mean)	RMSE (% of mean)	RMSE (% of mean)
H2O_M (ppm)	336			16%
RHw_M (%)	40			12%
O3_M (ppb)	80	3%	12%	6%
CO_M (ppb)	80	1%	8%	3%
CH4_M (ppb)	1850	<1%	<1%	<1%
NOx_M	64	-8%	44%	22%
NOxPSS_M	46	-17%	70%	25%
HNO3_M	162	-6%	22%	12%
HNO4_M	26	-7%	54%	28%
PAN_M	87	6%	25%	14%
CH2O_M	140	6%	22%	11%
H2O2_M	250	9%	30%	16%
CH3OOH_M	381	12%	45%	21%
Acetone_M	351	3%	18%	
Acetald_M	56	3%	19%	
C2H6_M	644	2%	16%	
C3H8_M	109	3%	16%	
iC4H10_M	11	6%	29%	
nC4H10_M	21	5%	29%	
Alkanes_M	16	3%	33%	
C2H4_M	6	28%	94%	
Alkenes_M	0.2	17%	78%	
C2H2_M	97	10%	42%	
C5H8_M	0.5	16%	70%	
Benzene_M	15	-12%	33%	
Toluene_M	1	4%	28%	
Xylene_M	0.1	33%	97%	
MeONO2_M	9	-11%	29%	
EtONO2_M	2	-11%	33%	
RONO2_M	5	-5%	37%	
MeOH_M	590	3%	38%	
HCN_M	185	5%	31%	10%
CH3CN_M	114	11%	44%	
SF6_M	9	<1%	1%	<1%

<b>Table S6. Test of missing flight data</b>			
Missing data (ppt unless noted)	All parcels Mean (ppt)	Interpolated RMSE (% of mean)	Flights used
<b><i>ATom-1 RF-5</i></b>			
H2O2_M	392	24%	AT-1 RF4, AT-2/3/4 RF-4/5
HNO3_M	139	58%	AT-1 RF4, AT-2/3/4 RF-4/5
HNO4_M	30.2	66%	AT-1 RF4, AT-2 RF-4/5
<b><i>ATom-2 RF-2</i></b>			
H2O2_M	125	23%	AT-2 RF-3, AT-1/3/4 RF-2/3
HNO3_M	30.9	52%	AT-2 RF-3, AT-1/3/4 RF-2/3
HNO4_M	14.3	63%	AT-2 RF-3, AT-1 RF-2/3
<b><i>ATom-3 RF-1</i></b>			
NOx_M	80.9	55%	AT-3 RF-2, AT-1/2/4 RF-1/2
<b><i>ATom-3/4 all</i></b>			
HNO4_M	26.1	105%	AT-1/2 all
<b><i>ATom-4 RF-5/6/7/8/9/12/13</i></b>			
CH3OOH_M	336	72%	AT-1/2 RF-5:11, AT-3 RF-5:13, AT-4 RF-4
Notes: Missing flight data are filled using a multiple linear regression from other flights based on the explanatory variables: pressure, noontime solar zenith angle, and latitude (in that order). RMSE is calculated from the residuals of this fit for the flights used in the regression.			

Used in	ID	Model name	Type	Meteorology	Model Grid	References	Point of Contact
clim	GFDL	GFDL-AM3	CCM	NCEP (nudged)	C180 x L48	Horowitz et al., 2003; Li et al. 2017	amfiore @ldeo.columbia.edu
clim, MDS-0	GISS	GISS-E2.1	CCM	Daily SSTs, nudged to MERRA	2° x 2.5° x 40L	Rienecker et al.,	lee.murray @rochester.edu
clim, MDS-0/1	GMI	GMI-CTM	CTM	MERRA	1° x 1.25° x 72L	Strahan et al., 2013; Duncan et al., 2007	Sarah.A.Strode @nasa.gov
clim, MDS-0	GC	GEOS-Chem	CTM	MERRA-2	2° x 2.5° x 72L	Gelaro et al., 2017	lee.murray @rochester.edu
clim, MDS-0	NCAR	CAM4-Chem	CCM	Nudged to MERRA	0.47° x 0.625° x 52L	Tilmes et al., 2016	emmons @ucar.edu
clim, MDS-0/1/2	UCI	UCI-CTM	CTM	ECMWF IFS Cy38r1	T159N80 x L60	Holmes et al., 2017; Prather 2015	mprather @uci.edu
MDS-0	F0AM	F0AM	box	MDS+scaled ATom Js	N/A	Wolfe et al., 2016	glenn.m.wolfe @nasa.gov
<p>The descriptions of models used in the paper. The first column denotes if the model's August climatology is used ('clim') and also the MDS versions used. F0AM used chemical mechanism MCMv331 plus J-HNO4 plus O1D)+CH4. For the global models see P2017, P2017, and H2018.</p>							

<b>Table S8a. Average Reactivities: mean, median, mean of top 10%</b>												
Value	Region	MDS-0							MDS-1	MDS-2		
		F0AM	GC	GISS	GMI	NCAR	UCI	U15	U97	GMI1	UCI2	UCI2*
P-O3, mean, ppb/d												
	Global	1.94	1.91	2.31	1.86	1.97	2.15	2.13	2.13	2.07	2.18	2.11
	Pacific	1.91	1.95	1.94	1.92	1.92	2.13	2.08	2.10	2.06	2.33	2.26
	Atlantic	1.88	1.99	3.29	2.07	2.28	2.32	2.32	2.34	2.22	2.08	2.02
P-O3, median, ppb/d												
	Global	1.28	1.43	1.69	1.35	1.47	1.53	1.50	1.51	1.58	1.58	1.54
	Pacific	1.31	1.64	1.60	1.48	1.56	1.66	1.63	1.65	1.72	1.99	1.93
	Atlantic	1.76	1.84	3.16	1.97	2.14	2.03	2.05	2.06	2.10	1.94	1.88
P-O3, mean of top 10%, ppb/d												
	Global	7.15	6.44	7.50	6.25	6.38	7.67	7.67	7.62	6.84	7.32	7.10
	Pacific	6.59	5.49	5.40	5.60	5.56	6.49	6.23	6.29	5.83	6.20	6.01
	Atlantic	4.63	5.18	7.97	5.49	5.74	6.53	6.53	6.61	5.55	5.26	5.10
L-O3, mean, ppb/d												
	Global	1.63	1.45	1.75	1.50	1.51	1.56	1.55	1.55	1.50	1.57	1.54
	Pacific	1.60	1.48	1.74	1.51	1.44	1.54	1.50	1.52	1.48	1.53	1.50
	Atlantic	2.06	1.90	2.23	2.04	2.28	2.14	2.14	2.16	2.04	2.15	2.11
L-O3, median, ppb/d												
	Global	0.87	0.85	1.11	0.83	0.86	0.89	0.88	0.88	0.81	0.90	0.88
	Pacific	1.00	0.99	1.23	0.98	0.98	1.04	1.07	1.04	0.91	1.03	1.01
	Atlantic	1.12	1.06	1.33	1.06	1.40	1.14	1.13	1.11	1.03	1.19	1.16
L-O3, mean of top 10%, ppb/d												
	Global	6.00	5.37	6.03	5.61	5.80	5.94	5.95	5.97	5.79	5.91	5.79
	Pacific	5.40	4.70	5.16	4.83	4.64	4.91	4.72	4.87	5.00	4.79	4.69
	Atlantic	5.96	5.88	6.62	6.24	7.89	6.67	6.70	6.76	6.20	6.55	6.41
L-CH4, mean, ppb/d												
	Global	0.72	0.66	0.38	0.65	0.62	0.68	0.68	0.68	0.67	0.68	0.68
	Pacific	0.81	0.78	0.38	0.76	0.73	0.79	0.77	0.78	0.77	0.79	0.79
	Atlantic	0.77	0.74	0.49	0.77	0.80	0.80	0.80	0.81	0.79	0.79	0.79
L-CH4, median, ppb/d												
	Global	0.36	0.37	0.29	0.34	0.34	0.36	0.36	0.36	0.37	0.38	0.38
	Pacific	0.48	0.56	0.35	0.51	0.46	0.54	0.55	0.54	0.54	0.60	0.60
	Atlantic	0.49	0.51	0.48	0.47	0.59	0.50	0.50	0.50	0.48	0.54	0.53
L-CH4, mean of top 10%, ppb/d												
	Global	2.55	2.18	1.09	2.21	2.12	2.40	2.38	2.40	2.33	2.28	2.27
	Pacific	2.66	2.24	1.00	2.29	2.19	2.35	2.27	2.31	2.36	2.16	2.15
	Atlantic	2.13	1.94	1.08	2.08	2.27	2.24	2.23	2.28	2.14	2.18	2.17
Global includes all ATom-1 parcels, Pacific considers all measurements over the Pacific Ocean from 54°S to 60°N, and Atlantic uses parcels from 54°S to 60°N over the Atlantic basin. All parcels are weighted inversely by the number of parcels in each 10° latitude by 100 hPa bin. Results from the different MDS versions (0, 1, 2) are shown. UCI2* uses the revised RDS* protocol that preprocesses the MDS-2 initializations with a 24-hour decay of HNO4 and PAN according to their local thermal decomposition frequencies, see text. See Table 2												

<b>Table S8b. Percent of total Reactivity in the top 50%, top 10%, top 3% of parcels</b>												
Value	Region	MDS-0								MDS-1	MDS-2	
		F0AM	GC	GISS	GMI	NCAR	UCI	U15	U97	GMI1	UCI2	UCI2*
P-O3, % of total R in top 50%												
	Global	85%	85%	83%	85%	85%	86%	86%	86%	84%	85%	85%
	Pacific	84%	81%	78%	82%	81%	82%	82%	82%	80%	80%	80%
	Atlantic	77%	81%	78%	80%	79%	80%	81%	81%	79%	81%	81%
P-O3, % of total R in top 10%												
	Global	37%	34%	32%	34%	32%	36%	36%	36%	33%	34%	34%
	Pacific	34%	28%	28%	29%	29%	31%	30%	30%	28%	27%	27%
	Atlantic	25%	26%	24%	27%	25%	28%	28%	28%	25%	25%	25%
P-O3, % of total R in top 3%												
	Global	18%	16%	15%	15%	15%	17%	17%	17%	15%	16%	16%
	Pacific	16%	11%	12%	12%	12%	13%	13%	13%	11%	11%	11%
	Atlantic	10%	11%	10%	11%	10%	12%	12%	13%	10%	10%	10%
L-O3, % of total R in top 50%												
	Global	88%	88%	87%	89%	88%	89%	89%	89%	89%	88%	88%
	Pacific	88%	87%	85%	87%	86%	87%	86%	86%	87%	87%	87%
	Atlantic	88%	88%	87%	89%	88%	89%	89%	89%	89%	89%	89%
L-O3, % of total R in top 10%												
	Global	37%	37%	35%	38%	38%	38%	39%	39%	39%	38%	38%
	Pacific	34%	32%	30%	32%	32%	32%	32%	32%	34%	31%	31%
	Atlantic	29%	31%	30%	31%	35%	31%	31%	31%	31%	31%	31%
L-O3, % of total R in top 3%												
	Global	15%	14%	14%	15%	17%	15%	15%	15%	15%	15%	15%
	Pacific	14%	13%	12%	14%	14%	13%	13%	13%	15%	13%	13%
	Atlantic	11%	11%	11%	11%	16%	12%	12%	11%	11%	11%	11%
L-CH4, % of total R in top 50%												
	Global	90%	90%	82%	91%	89%	91%	91%	91%	90%	89%	89%
	Pacific	90%	88%	79%	88%	87%	88%	88%	88%	87%	86%	86%
	Atlantic	86%	86%	77%	88%	86%	87%	87%	88%	87%	87%	87%
L-CH4, % of total R in top 10%												
	Global	36%	33%	29%	34%	34%	35%	35%	35%	35%	33%	33%
	Pacific	33%	29%	26%	30%	30%	30%	30%	30%	31%	27%	27%
	Atlantic	28%	26%	22%	27%	28%	28%	28%	28%	27%	28%	28%
L-CH4, % of total R in top 3%												
	Global	15%	12%	12%	13%	13%	14%	14%	14%	13%	13%	13%
	Pacific	14%	11%	11%	11%	11%	12%	12%	12%	11%	11%	11%
	Atlantic	10%	9%	8%	9%	10%	10%	10%	10%	10%	10%	10%

438  
439

See Table S8a.

440

Value	Region	MDS-0							MDS-1	MDS-2		
		F0AM	GC	GISS	GMI	NCAR	UCI	U15	U97	GMI1	UCI2	UCI2*
J-O1D, mean, e-5 /s												
	Global	1.14	0.97	1.48	1.03	1.09	1.01	1.00	1.01	1.04	1.00	1.00
	Pacific	1.31	1.19	1.76	1.25	1.29	1.24	1.22	1.23	1.25	1.21	1.21
	Atlantic	1.27	1.10	1.53	1.18	1.36	1.19	1.19	1.19	1.19	1.18	1.18
J-NO2, mean, e-3 /s												
	Global	4.57	4.28	5.48	4.23	4.40	4.68	4.62	4.62	4.27	4.63	4.63
	Pacific	4.51	4.43	5.47	4.36	4.54	4.84	4.77	4.82	4.35	4.77	4.77
	Atlantic	4.52	4.30	5.09	4.29	4.48	4.80	4.79	4.82	4.32	4.77	4.77

441

See Table S8a.

442

443

	P-O3	L-O3	L-CH4	J-O1D	J-NO2
GC	11%	9%	10%	9%	9%
GISS	22%	14%	17%	14%	12%
GMI	10%	9%	10%	10%	10%
NCAR	23%	32%	28%	17%	16%
UCI	10%	10%	11%	10%	11%

444

445

446 **SI References**

447

448 Duncan, B.N., Logan, J.A., Bey, I., Megretskaia, I.A., Yantosca, R.M., Novelli, P.C.,  
449 Jones, N.B. and Rinsland, C.P., 2007. Global budget of CO, 1988–1997: Source  
450 estimates and validation with a global model. *Journal of Geophysical Research:*  
451 *Atmospheres*, 112(D22).

452

453 Gelaro, R., McCarty, W., Suárez, M.J., Todling, R., Molod, A., Takacs, L., Randles,  
454 C.A., Darmenov, A., Bosilovich, M.G., Reichle, R. and Wargan, K., 2017. The modern-  
455 era retrospective analysis for research and applications, version 2 (MERRA-2). *Journal of*  
456 *climate*, 30(14), pp.5419-5454.

457

458 Holmes, C.D. and Prather, M.J., 2017. An atmospheric definition of the equator and its  
459 implications for atmospheric chemistry and climate. *Nature Geoscience*.

460

461 Horowitz, L.W., Walters, S., Mauzerall, D.L., Emmons, L.K., Rasch, P.J., Granier, C.,  
462 Tie, X., Lamarque, J.F., Schultz, M.G., Tyndall, G.S. and Orlando, J.J., 2003. A global  
463 simulation of tropospheric ozone and related tracers: Description and evaluation of  
464 MOZART, version 2. *Journal of geophysical research: Atmospheres*, 108(D24).

465

466 Li, D., Zhang, R. and Knutson, T.R., 2017. On the discrepancy between observed and  
467 CMIP5 multi-model simulated Barents Sea winter sea ice decline. *Nature*  
468 *Communications*, 8(1), pp.1-7.

469

470 Prather, M.J., Zhu, X., Flynn, C.M., Strode, S.A., Rodriguez, J.M., Steenrod, S.D., Liu,  
471 J., Lamarque, J.F., Fiore, A.M., Horowitz, L.W. and Mao, J., 2017. Global atmospheric  
472 chemistry—which air matters. *Atmospheric Chemistry and Physics*, 17(14), pp.9081-9102.

473

474 Prather, M.J., Flynn, C.M., Zhu, X., Steenrod, S.D., Strode, S.A., Fiore, A.M., Correa,  
475 G., Murray, L.T. and Lamarque, J.F., 2018. How well can global chemistry models  
476 calculate the reactivity of short-lived greenhouse gases in the remote troposphere,  
477 knowing the chemical composition. *Atmospheric Measurement Techniques*, 11(5),  
478 pp.2653-2668.

479

480 Rienecker, M.M., Suarez, M.J., Gelaro, R., Todling, R., Bacmeister, J., Liu, E.,  
481 Bosilovich, M.G., Schubert, S.D., Takacs, L., Kim, G.K. and Bloom, S., 2011. MERRA:  
482 NASA's modern-era retrospective analysis for research and applications. *Journal of*  
483 *climate*, 24(14), pp.3624-3648.

484

485 Strahan, S.E., Douglass, A.R. and Steenrod, S.D., 2016. Chemical and dynamical impacts  
486 of stratospheric sudden warmings on Arctic ozone variability. *Journal of Geophysical*  
487 *Research: Atmospheres*, 121(19), pp.11-836.

488

489 Tilmes, S., Sanderson, B.M. and O'Neill, B.C., 2016. Climate impacts of geoengineering  
490 in a delayed mitigation scenario. *Geophysical Research Letters*, 43(15), pp.8222-8229.

491



492 Wofsy, S.C., Afshar, S., Allen, H.M., Apel, E.C., Asher, E.C., Barletta, B., Bent, J., Bian,  
493 H., Biggs, B.C., Blake, D.R. and Blake, N., 2018. ATom: Merged atmospheric chemistry,  
494 trace gases, and aerosols. ORNL DAAC Oak Ridge, Tennessee, USA.  
495  
496 Wolfe, G.M., Marvin, M.R., Roberts, S.J., Travis, K.R. and Liao, J., 2016. The  
497 framework for 0-D atmospheric modeling (FOAM) v3. 1. Geoscientific Model  
498 Development, 9(9), pp.3309-3319.